LOW ACTIVITY MÖSSBAUER SOURCES FOR UNDERGRADUATE LABS

By

Keith W. Mann

A thesis submitted in partial fulfillment of the
requirements for the degree of

Bachelor of Science

Houghton College

July 2013

Signature of Author……..……..
Department of Physics
July 18, 2013

……..
Dr. Mark Yuly
Professor of Physics and Department Chair
Research Supervisor

……..
Dr. D. Brandon Hoffman
Associate Professor of Physics

LOW ACTIVITY MÖSSBAUER SOURCES FOR UNDERGRADUATE LABS

By

Keith M. Mann

Submitted to the Department of Physics
on July 18, 2013 in partial fulfillment of the
requirement for the degree of
Bachelor of Science

Abstract

Mössbauer experiments for undergraduates typically use radioactive sources measured in mCi, which excludes small institutions that do not have radioactive source licenses. In response to this need, we are developing a technique for producing inexpensive, low-activity, license-exempt Mössbauer sources. Cobalt in a solution of $CoCl_2$ in HCl containing approximately 1 μCi of ^{57}Co will be electroplated to a stainless steel foil and subsequently heated in a vacuum to about 1000°C to allow the ^{57}Co atoms to permeate the crystal lattice of the steel substrate. Several different methods of measuring the temperature have been tested in order to ensure that the foil is heated to the optimal temperature. Once created, these radioactive sources will be tested using a standard Mössbauer apparatus with the long-term intention of using the Mössbauer effect to measure the transverse Doppler shift due to relativistic effects as an undergraduate lab.

Thesis Supervisor: Dr. Mark Yuly
Title: Professor of Physics and Department Chair

TABLE OF CONTENTS

TABLE OF FIGURES

Chapter 1

THE MÖSSBAUER EFFECT

1.1 Discovery

The discovery of the Mössbauer effect was born out of the study of atomic resonance fluorescence, which began soon after the turn of the nineteenth century. To understand resonance fluorescence, consider an atom transitioning from the ground state to an excited state by absorbing a certain amount of energy, E_T. By emitting a photon with an energy equivalent to the transition energy E_T, it can revert back to its ground state. Provided that the energy of the photon is close enough to the energy of the transition, another atom of the same type can absorb this photon, and repeat the process.

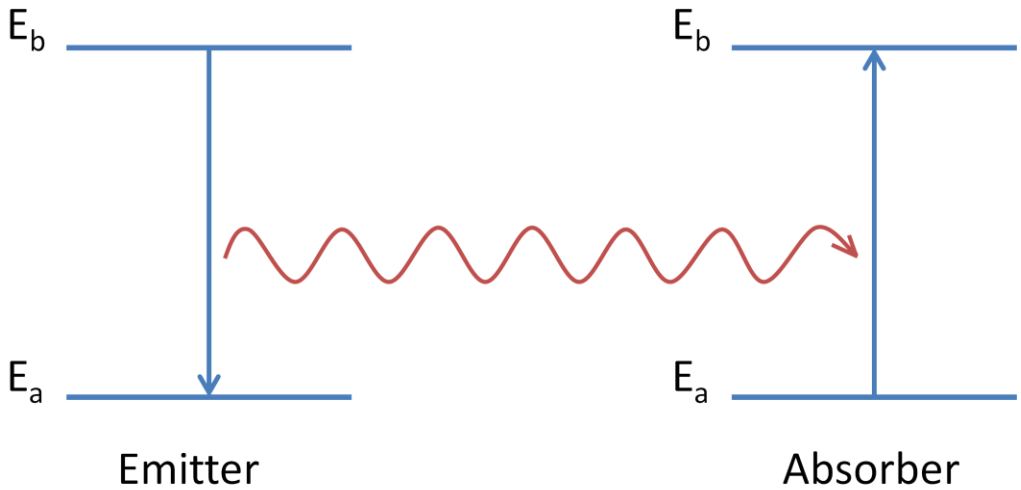

Figure 1: An emitting body transitions from excited state E_b to ground state E_a by emitting a photon with an energy equal to the energy difference between states E_a and E_b. The absorbing body can absorb this same photon so that it is excited from its ground state E_a to an excited state E_b.

Atomic resonance fluorescence was first observed in gaseous sodium by Gustav Wiedemann in 1904, and later confirmed by an American physicist Robert Wood [1]. In Wood's experiment, an iron tube was sealed off at both ends by glass plates, and a viewing window was on the side. In front of one glass plate, a lens was placed outside of the tube so that the focal point of the sunlight passing through the lens was inside of the apparatus. A Bunsen burner was placed directly below a container holding a sample of solid sodium that was inside of the tube so that when the container was heated, the chamber was filled with sodium gas. When the sunlight was incident on the gaseous sodium, the gas fluoresced with a green light near the focal point. In addition to this, Wood observed the fact that the alignment of the emission and absorption lines for sodium matched up precisely, but couldn't say conclusively why this was the case. Wood's observation of the overlap of the absorption and emission lines for sodium was the first evidence for atomic resonance fluorescence.

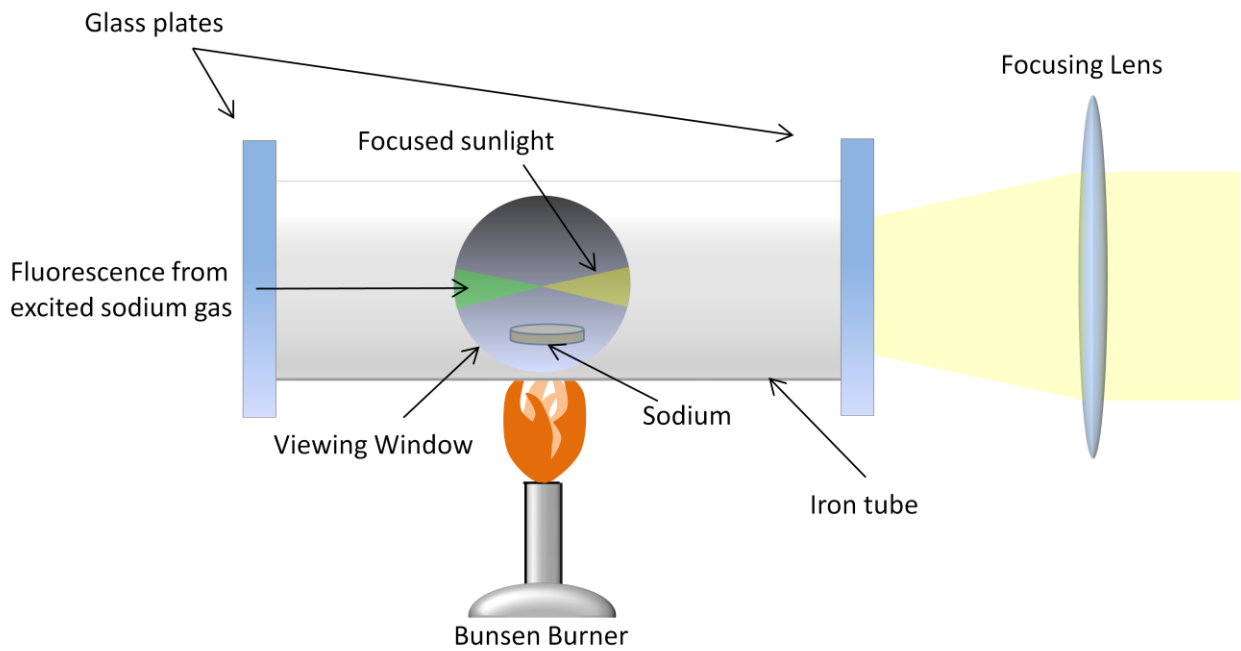

Figure 2: A representation of Wood's apparatus for observing atomic resonance fluorescence in sodium. A Bunsen burner heats the solid sodium to release sodium gas within the iron tube. Sunlight is focused into the iron tube by the focusing lens, and excites the sodium so that it fluoresces.

This observation of atomic resonance fluorescence led physicists to wonder if a similar phenomenon could be seen for photons with much higher energy than visible light, such as gamma radiation. Unfortunately though, experiments attempting to observe this phenomenon were unsuccessful for several decades.

After one such experiment, Swiss chemist Werner Kuhn conjectured [2] that there were three key elements that needed to be further explored in order to solve the resonance fluorescence mystery; namely, Doppler broadening due to thermal energy, additional broadening as the result of beta particle emission, and the red-shift of the emitted gamma ray. It was known by this time that photons had momentum; however, Kuhn hypothesized that for cases where gamma radiation was emitted, the energy of the outgoing photon was large enough so that the energy shift due to recoil made the absorption and emission lines no longer overlap enough to observe resonance fluorescence.

By 1950, there had been two semi-successful approaches [3, 4] to observing nuclear resonance fluorescence by compensating for the energy lost by the gamma ray due to recoil. In one of these experiments, a gamma emitter was placed on a spinning rotor. This was done so that when the source was moving towards the absorbing body, the emitted photons were blue-shifted relative to the absorber, cancelling out the effect of recoil at the moment of emission. In the second experiment, Karl Malmfors attempted to observe resonance by taking advantage of Doppler broadening by heating the source. As the gamma emitter was heated, the distribution of energies for the emitted radiation was widened to the point where resonance could be observed. Unfortunately, even though both of these experiments seemed to indicate signs of nuclear resonance fluorescence, the results were not statistically significant. Further experimentation would have to be done in order to confirm the observation of this phenomenon.

Soon after these experiments had been performed, Rudolf Mössbauer, a young German physicist, was attempting to replicate Malmfors' experiment for his doctoral work [5]. Instead of heating up the source as in Malmfors' experiment however, Mössbauer decided to decrease the temperature of the

source in anticipation of observing a decreasing overlap between the emission and absorption energy distributions. As the source began to approach the boiling point of nitrogen (~77K) however, Mössbauer began to notice an effect opposite to that which he had anticipated. Instead of the overlap decreasing, as was expected, it increased!

Eventually, Mössbauer determined that the cause of this unexpected result was the recoil-less emission of gamma rays. He deduced that when the gamma emitter had been cooled to a certain point, the recoil energy was transmitted to the crystal lattice as a whole rather than the recoiling nucleus. In order to explain how this would cause recoil-less emission of radiation, Mössbauer gave an analogy of someone throwing a rock while standing in a boat. As the rock is thrown, the majority of the energy goes into accelerating the rock towards the thrower's target, while a small portion of the energy manifests itself in the recoil of the boat. Because of this, the thrower is unable to throw as far on a boat as he would be able to on land. However, if the lake happened to be frozen while the rock is thrown, then the entire lake would absorb the recoil so that the thrower would have the ability to toss the rock just as far while standing in the boat.

In a similar fashion, when the nuclei emitting gamma rays are free to move, the energy loss due to recoil is significant enough so that resonance is not observed; however, if the decaying nuclei are anchored to other nuclei, then the recoil is distributed to all of the other atoms within the lattice, reducing the energy lost by the gamma ray to recoil, which in turn increases the likelihood of observing resonance.

Just after he had published his work on recoil-less gamma emission, Mössbauer realized the possibility of using the Doppler effect to explore nuclear resonance fluorescence further. To do this, he constructed another apparatus which consisted of a gamma source secured to the edge of a rotating disk. This disk was rotated so that the source was moving towards the absorber during the moment at which it was also in line with a Geiger counter. Thus, by varying the speed of the disk, Mössbauer

could determine the absorption of the gamma radiation as a function of rotational velocity, and the first Mössbauer spectrum was observed [5].

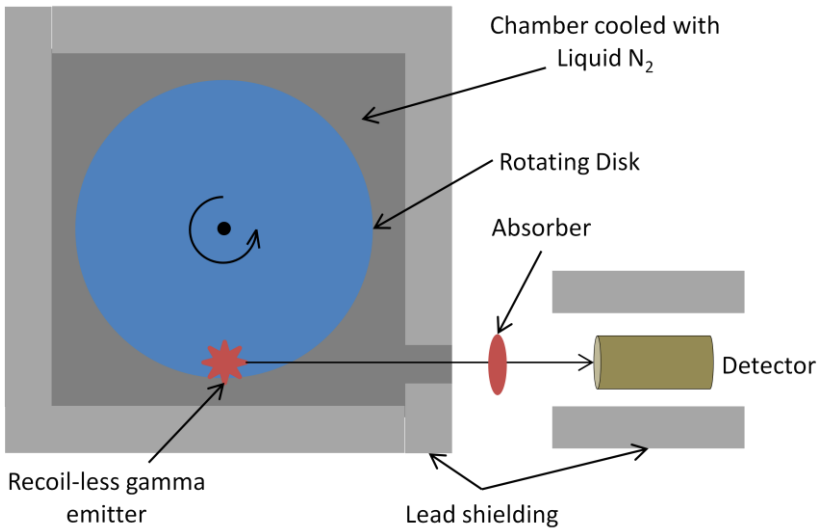

Figure 3: A depiction of the apparatus that Mössbauer used to collect the first Mössbauer spectrum. The chamber holding the source and the rotating disk was cooled with liquid nitrogen to minimize the energy loss of the gamma ray due to recoil. By varying the rotational velocity of the disk, a plot showing the number of events detected as a function of source velocity was able to be constructed.

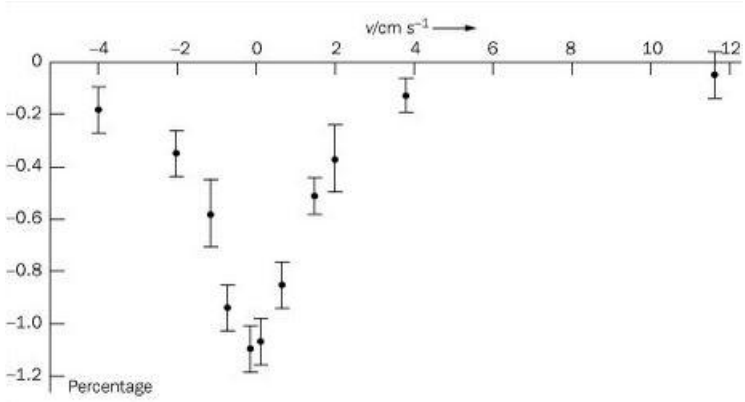

Figure 4: The first Mössbauer spectrum, collected by using an ^{191}Ir absorber, and an apparatus similar to the one shown in the previous figure. The plot depicts the percent of radiation absorbed as a function of the tangential velocity of the source. Figure taken from Ref. [5].

1.2 Using the Mössbauer Effect to Test General Relativity

The discovery of recoil-less gamma emitters provided an opportunity to test Einstein's theory of general relativity more precisely than ever before, with one particular experiment [6] even measuring to within one percent uncertainty.

One of these experiments was done by Robert Pound and Glen Rebka, a professor-student team at Harvard University in 1960. In their experiment, they placed a ^{57}Co source at the top of a vacant tower seventy-four feet tall and an absorber enriched with roughly thirty percent ^{57}Fe at the bottom of the same tower, with thermocouples monitoring the temperatures of both. A Mylar bag filled with flowing helium reduced the absorption of the gamma radiation. The source was oscillated by an electric transducer driven by a sinusoidal wave, and gated so that the data collected during the wave rise time was stored separately from the data collected during its fall time. An identical circuit was used to collect the data from a sodium-iodide detector in the same manner, and after a few data sets had been collected, the positions of the source and absorber/ detector were switched.

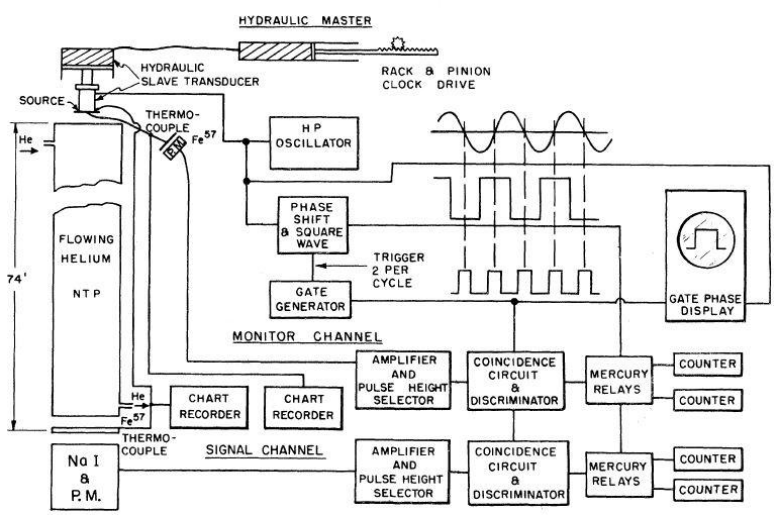

Figure 5: The apparatus and circuit diagram from Pound and Rebka's Experiment [7]. The source is moved by an electric transducer driven by a sinusoidal wave, and the circuit is set up to separate the data into two sections, based on whether it was collected during the rise or fall time of the wave. Figure taken from Ref. [7]

The frequency shift of the radiation emitted from the source was calculated by dividing the frequency of the outgoing gamma ray by the frequency of the photon that was absorbed. In addition, differences in temperature between the source and the detector were accounted for by using the data collected from the thermocouples.

Through this experiment they hoped to observe gravitational red-shifting and blue-shifting between the source and the detector—effects predicted by general relativity. Indeed, the frequency shift they measured with their apparatus was $(-5.13 \pm 0.10) \cdot 10^{-15}$, which compared well with the predicted value of $-4.92 \cdot 10^{-15}$ [7].

Table 1: One of the published data sets taken during Pound and Rebka's experiment. The above chart depicts the ratio of the source and absorber frequencies times 10^{15}. The corrections to the observed frequency shift calculated from the temperature differences were listed and accounted for in the calculation of the net shift. Table taken from Ref. [7].

Period	Shift observed	Temperature correction	Net shift
	Source at bottom		
Feb. 22, 5 p.m.	-11.5 ± 3.0	-9.2	-20.7 ± 3.0
	-16.4 ± 2.2[a]	-5.9	-22.3 ± 2.2
	-13.8 ± 1.3	-5.3	-19.1 ± 1.3
	-11.9 ± 2.1[a]	-8.0	-19.9 ± 2.1
	-8.7 ± 2.0[a]	-10.5	-19.2 ± 2.0
Feb. 23, 10 p.m.	-10.5 ± 2.0	-10.6	-21.0 ± 2.0
		Weighted average =	-19.7 ± 0.8
	Source at top		
Feb. 24, 0 a.m.	-12.0 ± 4.1	-8.6	-20.6 ± 4.1
	-5.7 ± 1.4	-9.6	-15.3 ± 1.4
	-7.4 ± 2.1[a]	-7.4	-14.8 ± 2.1
	-6.5 ± 2.1[a]	-5.8	-12.3 ± 2.1
	-13.9 ± 3.1[a]	-7.5	-21.4 ± 3.1
	-6.6 ± 3.0	-5.7	-12.3 ± 3.0
Feb. 25, 6 p.m.	-6.5 ± 2.0[a]	-8.9	-15.4 ± 2.0
	-10.0 ± 2.6	-7.9	-17.9 ± 2.6
		Weighted average =	-15.5 ± 0.8
		Mean shift =	-17.6 ± 0.6
		Difference of averages =	-4.2 ± 1.1

[a]These data were taken simultaneously with a sensitivity calibration.

In another experiment [6], Walter Kündig attached a Mössbauer source to a piezoelectric crystal, which was placed at the center of a hollow tube. An absorber was placed on one end of the tube, while a counterweight was placed on the other end so that the apparatus remained balanced. The piezoelectric crystal was driven by a function generator so that the speed of the source towards or away from the absorber could be controlled by the amplitude of the incoming signal.

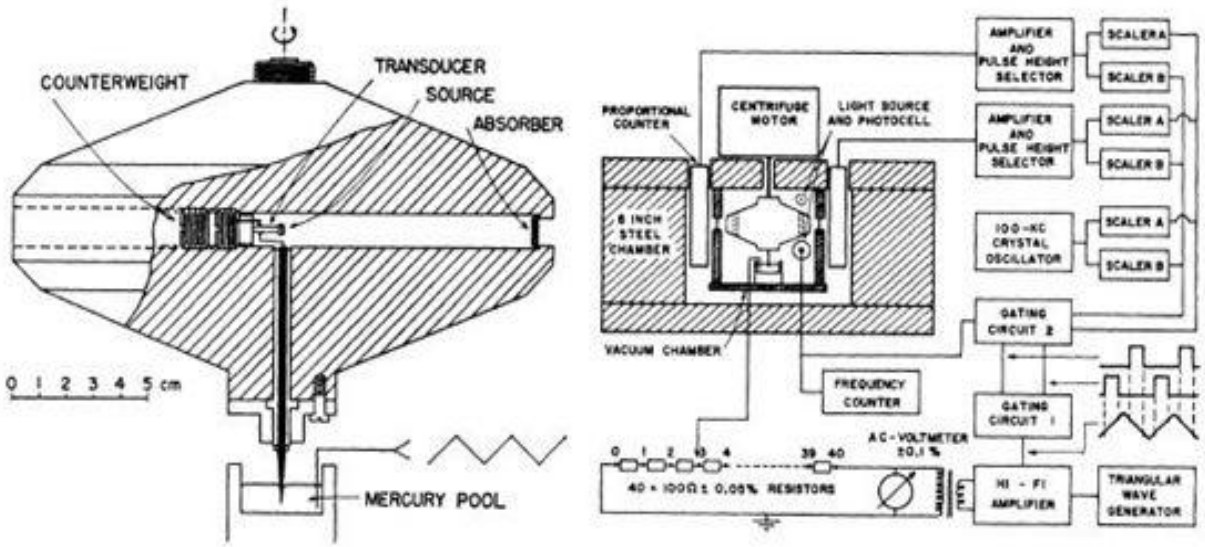

Figure 6: Drawing of Kündig's apparatus, along with the circuit diagram for the detector and piezoelectric. A Mössbauer source is mounted on a piezoelectric transducer at the center of the hollow, rotating cylinder. A counterweight is placed on one side of the cylinder to compensate for the absorber placed on the opposite end. The transducer is driven by a triangular wave from the function generator, which moves the source in and out relative to the absorber. When the cylinder is rotated, the source pivots with the absorber so that they are held in the same inertial reference frame while the absorber is under acceleration. Figure taken from Ref. [6].

Thus, if the apparatus remained stationary while the piezoelectric was driven with a triangle wave, a spectrum similar to the one Mössbauer collected in his experiment could be measured by varying the speed of the source. However, when the apparatus was rotated at a high angular velocity, the absorber

at the edge of the hollow tube experienced significant radial acceleration, while the acceleration that the source experienced at the center of the tube was negligible in comparison. Consequently, according to the equivalence principle of General relativity, the radiation incident onto the absorber was blue-shifted, which in turn moved the resonance peak away from the origin, in Kündig's results below.

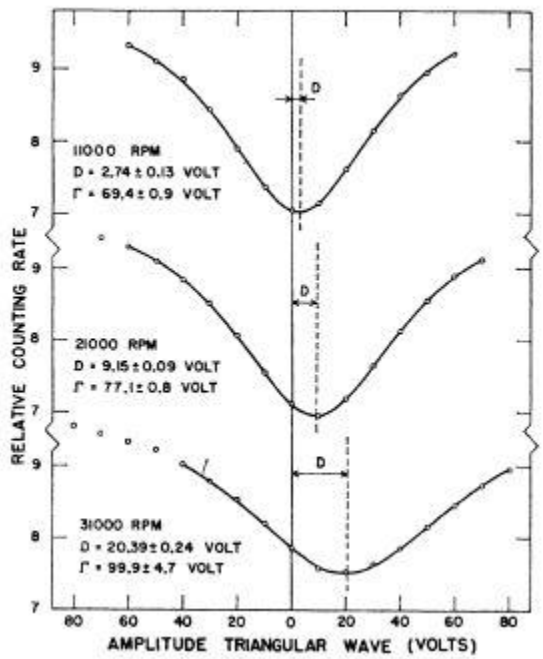

Figure 7: A typical plot of the relative counting rate of gamma rays as a function of the velocity of the source relative to the absorber (given by the amplitude of the triangular wave), for three different rotational speeds. As the speed of rotation increases, the distance *D* that the absorption peak (pointed out above by the dashed vertical line) is separated from zero increases, and the absorption peaks broaden. Figure taken from Ref [6].

Over forty years after Kündig's experimental results had been published, Kholmetskii et. al. [8] decided to analyze Kündig's results. The second-order correction of the relativistic energy shift due to the velocity of the source relative to the absorber is

$$\frac{\Delta E}{E} = k\frac{v^2}{c^2} \tag{1.2.1}$$

where v is the source velocity, c is the speed of light, and k is the second-order correction coefficient equal to 0.5. However, it was determined that if this equation was applied to the data gathered from Kündig's experiment and solved for k, the value was found to be 0.596—nearly twenty percent greater than the predicted value. Because of this discrepancy, Kholmetskii et. al. decided to construct an apparatus similar to Kündig's, and measure the absorption of gamma rays as a function of rotational speed.

The Kholmetskii et. al. apparatus was a tube made of an aluminum alloy seated inside of a chamber that was slightly larger than the tube so that it was free to rotate inside of the chamber. A Mössbauer source was placed at the center of the tube, while the absorber was placed directly outside of the tube so that it always faced the source as the tube was rotated. A detector was placed outside of a beryllium window that was attached to the chamber to count the number of gamma rays passing through the absorber. In addition, a collimator was placed in the tube to reduce the number of background counts, and the chamber was evacuated to roughly one-eighth of an atmosphere before beginning the experiment. The tube was then rotated inside of the chamber at various rotational speeds to collect the absorption spectrum of the radiation as a function of absorber velocity.

The data that were collected in this manner were very intriguing; the resonance curves measured did not seem to match the curve predicted by using the value $k = 0.5$. In order to better understand what was transpiring, theory curves derived using different values of k were plotted alongside the measured resonance curve. From this comparison, it was determined that $k = 0.68$ best fit the experimental data, which seemed to indicate the possibility that an effect other than general relativity was influencing the experimental outcome [8].

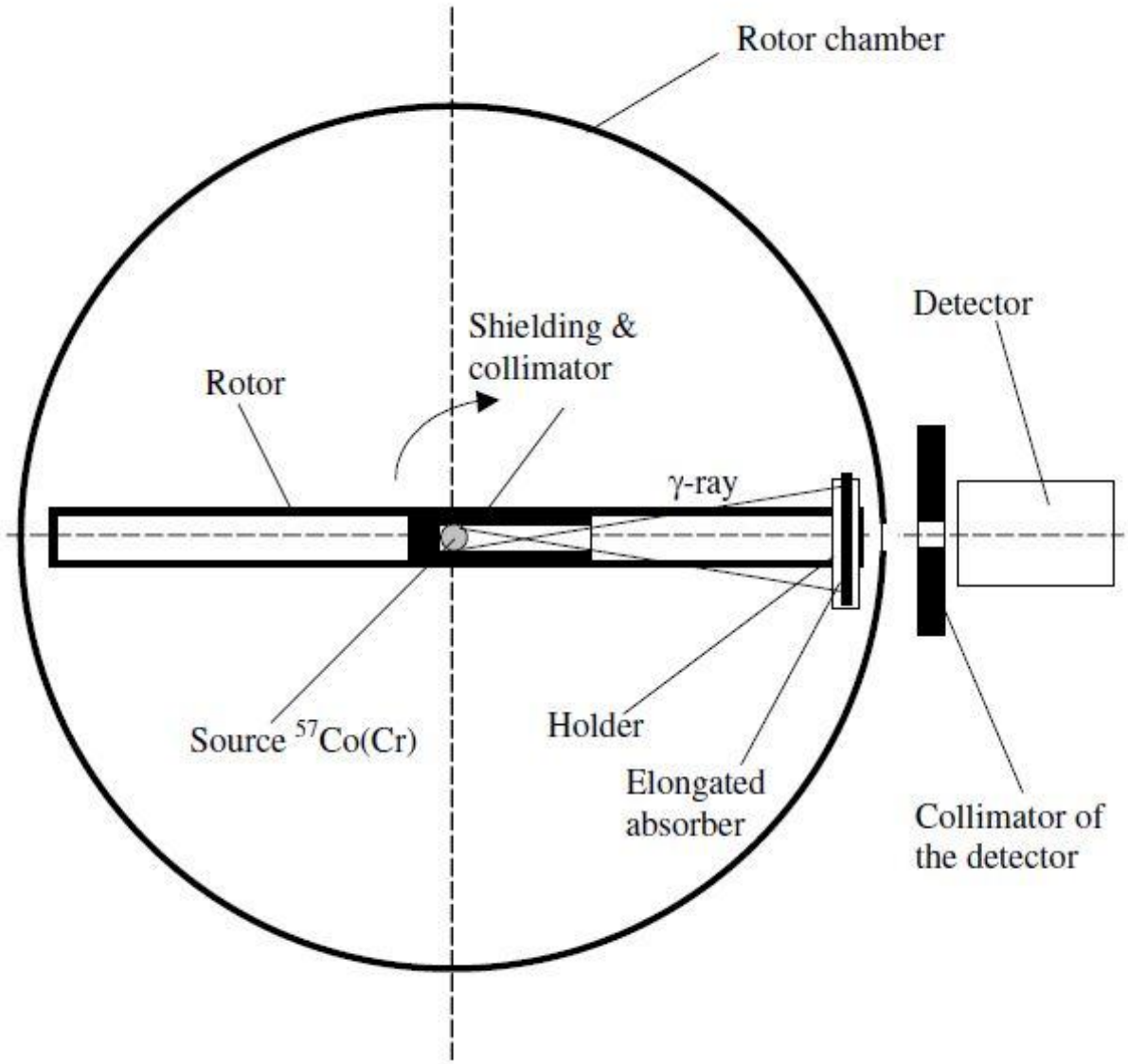

\

Figure 8: A sketch of the experimental setup used by Kholmetskii. The source, shielding, and absorber are all attached to the rotor, which is placed inside of the rotor chamber. A NaI detector is placed directly in front of the viewing window of the chamber, and the rotor is rotated at a large enough velocity so that the transvers Doppler effect can be observed. Figure taken from Ref. [8].

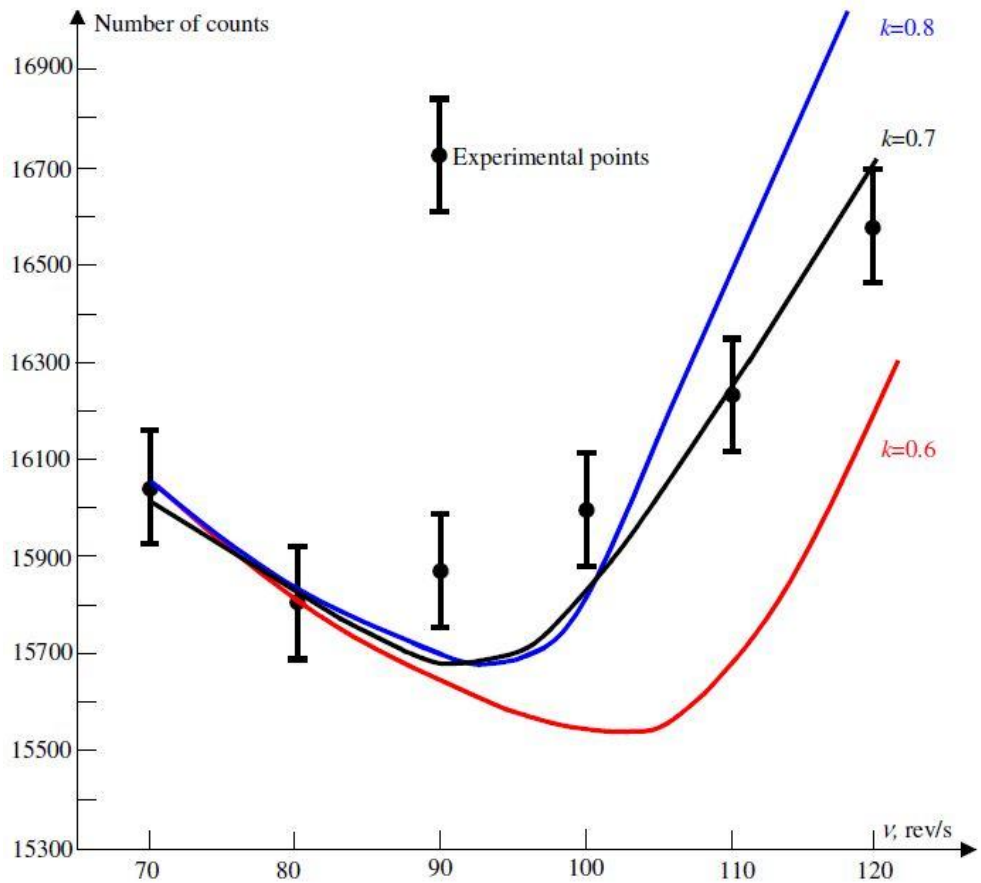

Figure 9: A plot comparing the measurements of Kholmetskii et. al. and theory curves calculated using different values of 'k'. Figure taken from Ref. [8].

1.3 Making Mössbauer Sources

Soon after Mössbauer assembled the first recoil-less gamma source, it became desirable to streamline the construction process to make them readily available for nuclear physics experiments. Several different methods of making recoil-less emitters have been published [8, 9, 10, 11, 12], with few common procedures that can be identified. For the purposes of this thesis, only methods for the construction of a Mössbauer source utilizing the 14.4 keV gamma rays from the decay of ^{57}Co will be described.

In general, the source material is first dissolved into a solution that is initially acidic, but is made more basic by adding ammonia until the pH of at least ten is reached. A substrate consisting of an iron foil that has been enriched with ^{57}Fe, which is resonant with the 14.4 keV gamma rays emitted from ^{57}Co is constructed. Next, the substrate is put into direct contact with the solution, and a fixed potential is set between the electroplating solution and the substrate. Lastly, the electroplated foil is heated to the annealing temperature of the substrate, usually in a vacuum chamber or in a hydrogen atmosphere, until the heat treatment is complete.

Table 2: Chart comparing the different electroplating methods described in the papers written by Mustachi, Stephen, Qaim, and Weicheng. Different solutions used to dissolve the source material, the pH of the solution before electroplating, the current density over the foil, and the approximate percent successfully electroplated for each method are shown. Data for this table taken from Ref. [8, 9, 10, 11, 12].

	Solution	**pH**	**Current Dens.** (mA/cm^2)	**% Yield**
Mustachi [9]	H_2SO_4	10 to 12	10mA/cm^2	80-90
Stephen [10]	$(NH_4)_3C_6H_5O_7$, $(NH_4)SO_4$, N_2H_5OH	above 10	100mA/cm^2	70-80% for <1µg, >99% for >1µg
Qaim [11]	HCl	about 12	20mA/cm^2	n/a
Weicheng [12]	N_2H_5OH, $(NH_4)_3C_6H_5O_7$	11 to 12	60mA/cm^2	85-97%
Bearden [13]	HCl	n/a	n/a	n/a

Table 3: Chart comparing the different methods employed for the heat treatment of the foil. The maximum temperature of the foil, the duration of the heating process, the pressure inside of the heating chamber, and the length of time over which the foil was cooled down are depicted. Data taken from Ref. [8, 9, 10, 11, 12].

	Treat Temp (^oC)	**Treat Time**	**Pressure**	**Cool Time**
Mustachi [9]	900 ^oC	2 hr	n/a	10 hr
Stephen [10]	1100 ^oC	12 to 50 hr (dep. on metal)	1 to 10 μTorr	(dep. on metal)
Qaim [11]	1200 ^oC	4 to 6 hr	n/a	n/a
Weicheng [12]	1000 ^oC	2 hr	n/a	n/a
Bearden [13]	1000 ^oC	2 hr	$< 10^{-6}$ mmHg	n/a

1.4 Previous Undergraduate Mössbauer Experiments

In addition to the experiment described in this thesis, other work has been done to investigate using the previous Mössbauer experiment at the undergraduate level. A couple of earlier experiments are worth mentioning; namely, those done by Bearden et. al. [13] and Sconza et. al. [14], as both experiments contribute uniquely to the discussion.

In Bearden et. al. [13], a 1mCi source was constructed in a fashion very similar to that which was reviewed in Section 1.3; ^{57}Co was electroplated to a stainless steel substrate, and subsequently heated to 1000^oC at an atmosphere of less than 1μTorr for two hours. The apparatus consisted of a Mössbauer

source in line with a sodium iodide detector with an absorber disk placed in between the two and tilted at an angle so that the axis of the disk was not in line with the source and detector. The disk was rotated at a fixed velocity for the duration of the data collection so that the absorber could be brought in and out of resonance with the source, dependent on its rotational velocity. Because the source and absorber possessed a finite size, the relative velocity of the absorber was different depending on at what angle the gamma ray was emitted from the source relative to the absorber. In order to accommodate this factor, the source was collimated, which allowed them to reduce the effect that this had on broadening the resonance peak.

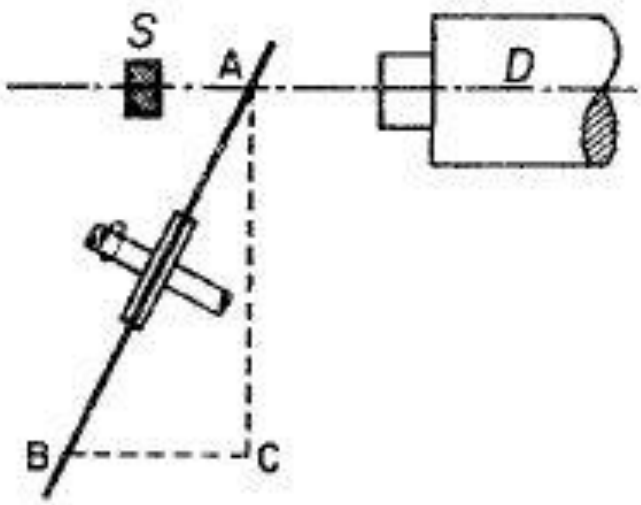

Figure 10: A schematic of Bearden's apparatus. Point A on the disk travels a distance BC, so that some component of the velocity is along the same line as the source S and the detector D. Figure taken from Ref. [13].

Sconza et. al. [14] utilized a source that had been donated from a Mössbauer research lab because its activity had dropped to a level which rendered it useless for experiments there. Since it still possessed approximately 1mCi of activity, Sconza was able to use it for his apparatus. Much like previous Mössbauer experiments, an absorber was placed in between the ^{57}Co source and a silicon diode detector. However, Sconza placed the absorber on a trolley that was driven at a constant velocity towards the source, instead of rotating the absorber disk as in Bearden et. al. apparatus.

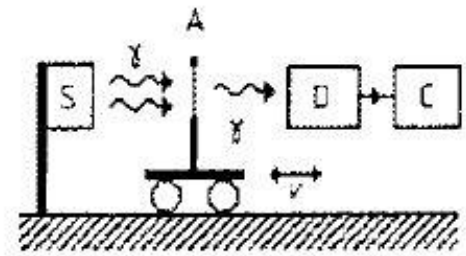

Figure 11: A depiction of Sconza's experimental arrangement. The absorber A is driven by a trolley with velocity v with respect to the source S. Some of the gamma rays that are not absorbed are observed by the detector D. Figure taken from Ref. [14].

1.5 Our Apparatus

The ultimate goal of this research is to use a recoil-less gamma emitter in conjunction with an apparatus that can be used to collect a Mössbauer spectrum in two different ways. The first method would implement the longitudinal Doppler effect—similar to Mössbauer's original design. An absorber disk would be set at angle relative to the source so that when the disk is rotated, a component of the disk's velocity will be in the same direction as the source, as shown in Figure 12. By varying the rotational speed of the absorber disk, the observed absorption as a function of relative source velocity could be determined. In addition, a coincidence measurement of two different types of gamma rays emitted from the source will be used to help reduce the background radiation. This process is discussed in detail in Section 3.5.

The second apparatus would have the absorber disk positioned so that it is completely perpendicular to the source, and rotating at high speed, similar to Kündig's experiment. Due to the radial acceleration, the absorber disk in an accelerated reference frame, and the incoming radiation would be blue-shifted, in accordance with the theory of general relativity. Because of this, the amount by which he gamma ray is blue shifted increases with greater acceleration. Consequently, by varying the angular

speed of the disk, the absorption as a function of rotational velocity could be determined, as shown in Figure 13.

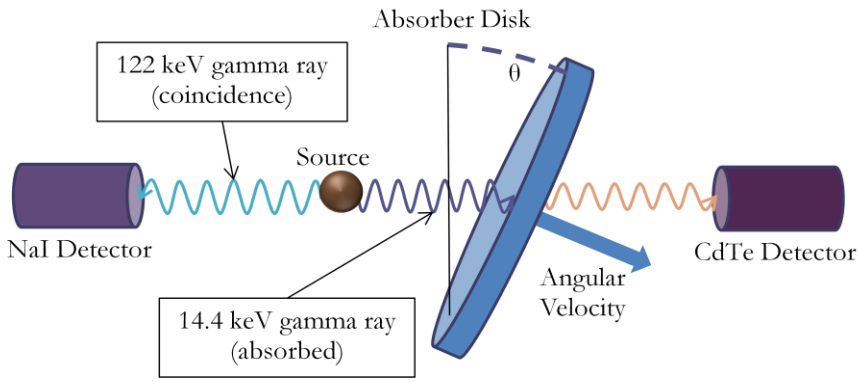

Figure 12: Depiction of proposed apparatus for using a Mössbauer source to observe the longitudinal Doppler effect. An absorber disk is tilted with an angle θ relative to the vertical, so that a component of the absorber's velocity is moving towards the source. By varying the rotational speed of the disk, a Mössbauer spectrum can be collected. 122 keV gamma rays are emitted simultaneously with the 14.4 keV gamma rays so that they can be detected in coincidence with one another. This process is explained in detail in Section 3.5.

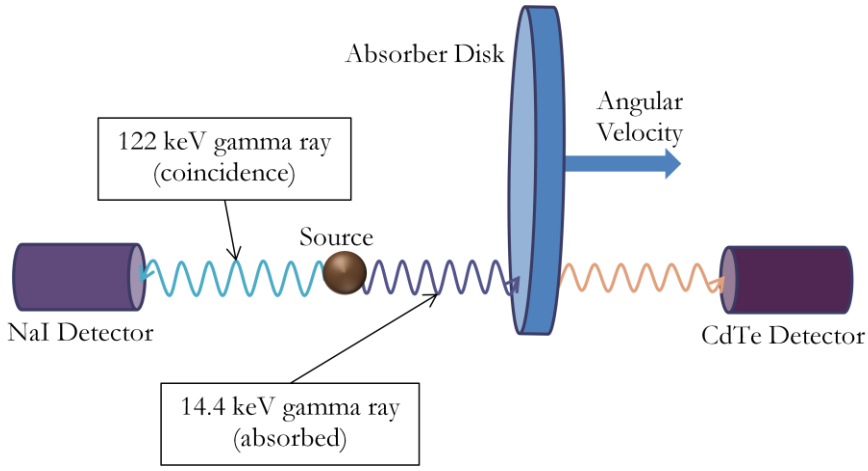

Figure 13: An apparatus similar to the one showed in Figure 12; however, the angle θ of the disk from the vertical has been reduced to zero so that the transverse Doppler effect can be observed.

Chapter 2

THEORY

2.1 Conservation of Momentum

Consider two identical nuclei; one of which is in an excited state while the other remains in the ground state. If the first of these nuclei reverts to its ground state by releasing a gamma ray, there is a possibility that the other nucleus can absorb the gamma ray and transition into an excited state. According to the conservation of momentum, however,

$$\left|\overrightarrow{P_R}\right| = \left|\overrightarrow{P_\gamma}\right|, \tag{2.1.1}$$

where $\overrightarrow{P_R}$ is the momentum of the recoiling nucleus and $\overrightarrow{P_\gamma}$ is the momentum of the gamma ray, and the two momenta are antiparallel to each other. From this equation it can be seen that if the recoiling body is less massive, then a larger portion of the gamma ray's energy will be imparted to the emitter atom. As a result, the emitted gamma ray experiences a Doppler shift such that energy of the emitted radiation is significantly less than the energy of the nuclear transition. Because of this Doppler shift, another nucleus of the same type will have a smaller probability of absorbing the gamma ray, causing the two nuclei to move out of resonance with each other.

2.2 Conservation of Energy

Let E_γ be the energy of the gamma ray emitted. Given that $E_\gamma = P_\gamma c$ for a photon, then according to the conservation of energy, the kinetic energy R imparted to the recoiling emitter nucleus is

$$R = \frac{P_R^2}{2M} = \frac{P_\gamma^2}{2M} = \frac{E_\gamma^2}{2Mc^2} \tag{2.2.1}$$

where Mc^2 is the rest mass of the recoiling nucleus. This assumes a non-relativistic interaction, which is safe, given that the nucleus is generally large enough so that only a very small percentage of the total energy from the outgoing photon is imparted to it.

The energies of the outgoing photon and recoil can be related to the energy of the transition, E_T by using conservation of energy

$$E_T = E_\gamma + R \tag{2.2.2}$$

Assume the recoil energy is small compared to the gamma ray energy, which is the case for low energy transitions in massive nuclei. Then, $R \ll E_\gamma$ so that $E_T \approx E_\gamma$. This means, using Eq. 2.2.1, that the recoil energy R can be approximated in terms of the transition energy

$$R \approx \frac{{E_T}^2}{2Mc^2} \tag{2.2.3}$$

However, this assumes that the emitter nucleus has no initial momentum before it emits the outgoing photon. Physically, this is not the case, as nuclei are constantly moving due to thermal energy, creating a Doppler broadening effect.

To account for this factor, let $\overrightarrow{P_I}$ be the initial momentum of the emitter nucleus, so that the momentum of the nucleus after emitting the gamma ray is equal to $\left(\overrightarrow{P_I} - \overrightarrow{P_\gamma}\right)$. Now, consider the recoil energy R' imparted to the nucleus,

$$R' = E_f - E_i \tag{2.2.4}$$

where E_i and E_f are the energies of the nucleus before and after emitting the gamma ray, respectively. If this is the case, then putting Eq. 2.2.4 in terms of momentum gives

$$R' = \frac{\left(\overrightarrow{P_I} - \overrightarrow{P_\gamma}\right)^2}{2M} - \frac{\overrightarrow{P_I}^2}{2M} \tag{2.2.5}$$

which can be simplified by expanding the first term.

$$R' = \frac{{P_I}^2}{2M} - \frac{2\overrightarrow{P_I} \cdot \overrightarrow{P_\gamma}}{2M} + \frac{{P_\gamma}^2}{2M} - \frac{\overrightarrow{P_I}^2}{2M} = \frac{\overrightarrow{P_\gamma}^2}{2M} - \frac{\overrightarrow{P_I} \cdot \overrightarrow{P_\gamma}}{M} \tag{2.2.6}$$

Now introduce the "Doppler energy," defined to be

$$D = 2(\varepsilon R)^{1/2} = 2\left(\frac{P_I^2}{2M} \cdot \frac{P_\gamma^2}{2M}\right)^{1/2} = \frac{P_I P_\gamma}{2M} \tag{2.2.7}$$

Hence,

$$\frac{\overrightarrow{P_I} \cdot \overrightarrow{P_\gamma}}{M} = D \cos\phi, \tag{2.2.8}$$

where ϕ is the angle between the momentum vectors $\overrightarrow{P_I}$ and $\overrightarrow{P_\gamma}$. Substituting this back into Equation 2.2.6 gives

$$R' = \frac{\overrightarrow{P_\gamma}^2}{2M} - D\cos\phi = R - D\cos\phi. \tag{2.2.9}$$

Consequently, accounting for Doppler broadening in Equation 2.2.2 and solving for E_γ gives

$$E_\gamma = E_T - R' = E_T - R + D\cos\phi \tag{2.2.10}$$

Clearly, from this result we see that the gamma ray energy $E\gamma$ is peaked at the energy

$$E_R = E_T - R$$

which is the transition energy shifted by the energy loss due to recoil. The term $D\cos\theta$ is responsible for the broadening, and has values ranging from $-D$ to $+D$.

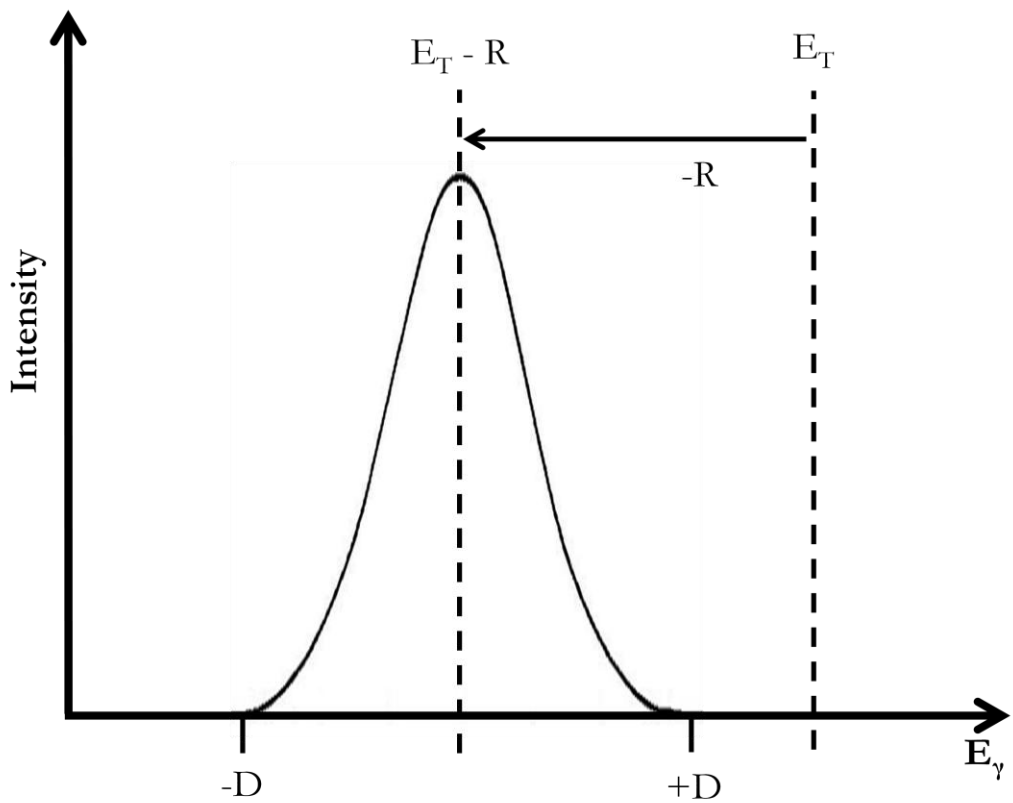

Figure 14: A plot of the probability intensity as a function of gamma ray energy E_γ for gamma rays with energy of E_T. The peak energy is located at E_T – R, due to the effects of Doppler broadening (from –D to +D) and the energy loss to recoil (-R).

2.3 Mean Line Width

Another factor contributing to the Mössbauer effect is the line width of the transition between two nuclear states. In fact, if the line width of the transition was zero, then the Mössbauer effect could never be observed because of the energy lost to the emitter nucleus due to recoil.

In other words, because of this small loss of energy, the outgoing gamma ray has less energy than the energy of the nuclear transition which precipitated it. Due to the Heisenberg uncertainty principle however,

$$\tau\Gamma = \hbar, \tag{2.3.11}$$

where τ is the mean life of the excited nuclear state, and Γ is the line-width, in terms of energy, of the de-excitation gamma rays. The line-width of this absorption depends on the nucleus, but is generally on the order of 10^{-6}eV [17].

As the result of Doppler broadening and the non-zero line width, the probability that an emitter atom will release a gamma ray of a given energy is a distribution centered about E_T, when energy losses due to recoil are not considered. From Equation 2.2.10, for a physical atom with finite mass, the energies of the emitted gamma ray are centered around $E_{\gamma i} = E_T - R$. In order for another nucleus of the same type to absorb an emitted photon, a gamma ray would have to possess an energy $E_{\gamma f} = E_T + R$ to compensate for the energy lost due to recoil to the absorber nucleus. In order for these two distributions to overlap, then

$$\Gamma > E_{\gamma f} - E_{\gamma i} = 2R. \tag{2.2.12}$$

As can be seen from Figure 16, the recoil energy R of the nucleus for smaller transition energies E_R are such that the requirement for overlap is met. However, when the energy of the transition approaches values within the energy range for gamma rays, it becomes extremely unlikely for overlap to occur. This explains why recoil-less resonance fluorescence was observed without much hindrance for photons within the range of visible light, but not with nuclear transitions.

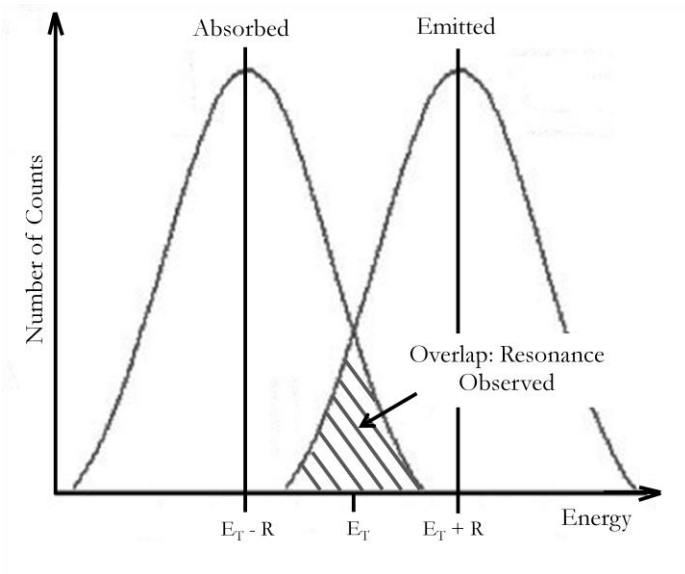

Figure 15: A plot showing the shift in energy of the gamma ray emitted from a nucleus transitioning from an excited state with energy E_T. The gamma ray transmits a portion of its energy R to the emitter and absorber, so that the difference between the two spectra is 2R. Nuclear resonance is observed when the two peaks overlap.

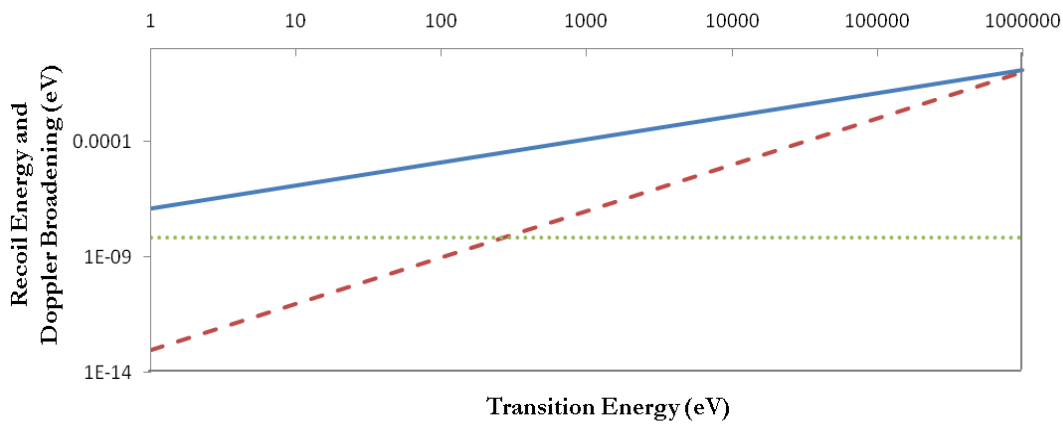

Figure 16: A plot depicting Doppler broadening and energy losses due to recoil (dashed orange line) as a function of transition energy for an ^{57}Fe atom. The Doppler broadening has been shown for 300K (solid blue line), and the mean line width for the transition (dotted green line) shown is from the most probable transition taken from the ^{57}Co decay chain (shown in Section 3.5). As the transition energy increases, the energy lost by the gamma ray due to recoil increases. Figure taken from Ref. [17].

2.4 What Makes a Good Absorber?

There are several important criteria to consider when deciding which element to use as an absorber material for use in a Mössbauer experiment. First of all, it is desirable for the mean lifetime of the transition to be low enough. For example, if the mean lifetime of the transition is on the order of hundredths of a nanosecond, even the tiniest bit of energy that is lost from the emitted gamma ray will result in a sizeable deviation from perfect resonance between the absorption and emission curves. An additional concern is the Mössbauer absorption cross section of the material. If an element possesses a desirable mean lifetime but has a small absorption cross section, then a larger quantity of the substance is required to produce the desired level of absorption. Yet another property desired from an absorber is a high abundance of the isotope, which inevitably corresponds with the cost of procuring the desired material. This becomes especially important when designing a Mössbauer experiment for small undergraduate laboratories.

The Mössbauer effect has been observed in a number of different nuclides. Many others meet one or more of the aforementioned criteria, but have other disadvantages. For example, ^{73}Ge has a desirable mean lifetime the order of microseconds, but has an absorption cross section of only $\sim 10^{-21}$ cm^2. ^{169}Tm has a sizeable cross section of $\sim 10^{-17}$ cm^2, but is the second most rare lanthanide on the periodic table. Although these absorbers are more extreme than usual, they represent the dilemma of balancing out the benefits with the disadvantages of each candidate. After comparing several different isotopes in this manner, ^{57}Fe was chosen since it composes 2.17% of the natural iron within the earth, which means that a stainless steel foil has enough of this isotope to be used as an absorber in a Mössbauer experiment. Of course, an iron sample enriched in ^{57}Fe could be used to enhance the observed effect further. In addition, it has a respectable absorption cross section of about 10^{-20} cm^2, and a mean lifetime of approximately one-tenth of a microsecond. (See Appendix A for table of different Mössbauer sources and their properties).

2.5 Calculating the Rotation Speed for the Absorber

Consider a gamma ray emitted from Mössbauer source with energy E. If the source is moved directly toward an absorber with velocity v, then any gamma rays it emits will experience an increase in energy, according to the approximation of the Doppler effect

$$E' = E\left(1 + \frac{v}{c} + \frac{v^2}{2c^2} + \cdots\right) \tag{2.5.1}$$

where E' is the new energy of the gamma ray. Because the source velocity necessary to measure a Mössbauer spectrum is generally on the order of $10^{-4}\ \mathrm{m}/\mathrm{s}$, the second order term is negligible for the purposes of this calculation. With this in mind, expanding the above formula gives

$$E' \cong E + \frac{Ev}{c} \tag{2.5.2}$$

From this equation the velocity necessary to shift the energy of the gamma ray by an amount ΔE is given by

$$v = \frac{c\Delta E}{E} \tag{2.5.3}$$

where $\Delta E = E' - E$ is the change in energy of the gamma ray due to the velocity of the source v.

Conversely, this concept can be applied to the absorber in order to determine the rotational velocity of the absorber disk. By using basic kinematics and trigonometry, the appropriate angular speed can be determined for given values of disk radius and angle of rotation.

Take for example, the experimental setup shown in Figure 12, with a disk of radius R, angular velocity ω, and an angular displacement θ with respect to the vertical. Given that the tangential velocity at any given point on the disk is $v = r\omega$ (where r represents a given distance from the center of the disk),

then the tangential velocity corresponding to the tilting angle θ is given by $v = R\omega \sin\theta$ for points on the edge of the disk. This means that the angular velocity of the source necessary to the energy of the gamma ray by some value ΔE is

$$\omega = \frac{c\Delta E}{ER\sin\theta} \quad . \tag{2.5.4}$$

Let R = 10 cm, θ = 45°, E = 14.4 keV, and ΔE = 10^{-7} eV; these parameters would be similar to what would be used if ^{57}Co was used as a Mössbauer source, and ^{57}Fe was used as an absorber. By substituting these into Equation 2.5.4, it can be seen that ω = 0.03 $^{\mathrm{cm}}/_{s}$.

Chapter 3

EXPERIMENTAL APPARATUS AND PROCEDURE

3.1 Making the Source

There are two main stages in making the source: depositing the source material onto the surface substrate, and embedding the source material into the crystal lattice of the substrate. A 1.27 cm by 2.59 cm by 0.005 cm thick piece of 321 stainless steel was used as a substrate. In order to begin the electroplating process, an apparatus was set up to deposit cobalt ions onto 321 grade stainless steel. Figure 17 shows the electroplating apparatus, which was a 'T' shaped glass tube, with one of the arms of the 'T' slightly raised upwards that the Co ion solution could be contained. This glass tee was placed in between two small rubber pads approximately the same length and width as the foil such that the stainless steel substrate separated the rubber pad from bottom end of the glass tube. This entire arrangement was compressed with a C-clamp secured to a ring stand.

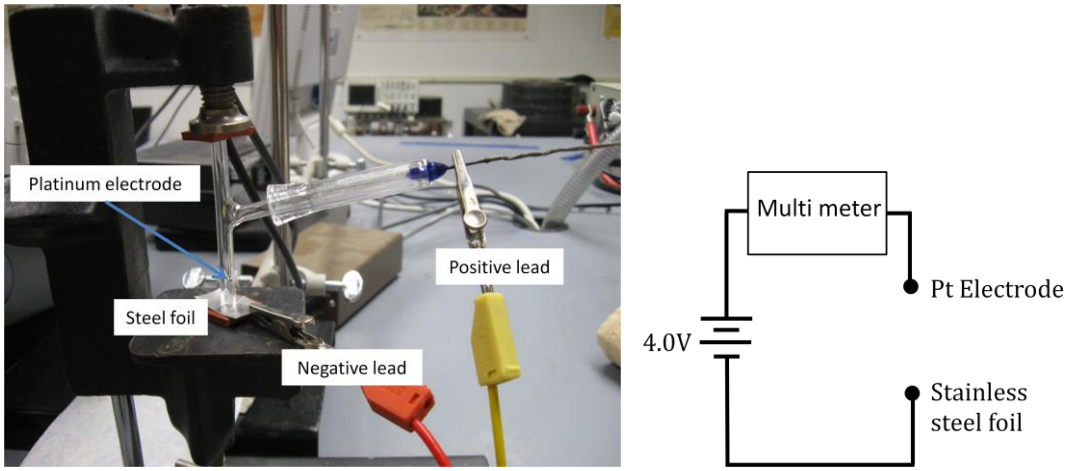

Figure 17: A photograph of the mechanism used to electroplate Cobalt ions to a stainless steel foil. A glass tube containing the solution with Cobalt ions was set on top of the steel foil and secured between two rubber pads using a C-clamp. A platinum-plated electrode is suspended within the Cobalt solution, and 4.0V of potential are set between the electrode and the foil to begin the electroplating process, and the current as a function of time was monitored by a RSR MS8050 multi meter.

Before beginning the electroplating process, the mass of the stainless steel foil was measured to $\pm 10^{-4}$ grams after cleaning the foil with distilled water. A 5mL 0.1M solution of HCl was prepared, and the initial mass of the HCl solution was measured. In order to begin electroplating, approximately ½mL of the 0.1M HCl solution was placed inside the glass tube, and a platinum-plated electrode was suspended inside the solution so that its end was positioned directly above the foil. Once this setup was complete, a 4.0V potential was placed between the platinum electrode and the foil, in accordance with the circuit diagram shown in Figure 17. The current as a function of time was then monitored for half an hour so that the current corresponding to the disassociation of the 0.1M HCl solution could be determined, as shown in Figure 18. Next, the mass of the remaining HCl solution was measured before a small amount (~0.1 g) of $^{59}CoCl_2 \cdot 6H_2O$ was placed into the remaining HCl solution with a pipette. After the $^{59}CoCl_2 \cdot 6H_2O$ was dissolved into the HCl, it was weighed so that the number of ^{59}Co atoms could be determined. This was done by determining the difference in mass before and after the $^{59}CoCl_2 \cdot 6H_2O$ was added, and using stoichiometry to determine the corresponding mass of the ^{59}Co. Once the electroplating process was complete, the entire apparatus was thoroughly cleaned: including the pipette, glass tee, and the electrode. This was done by rinsing each part methodically with distilled water and drying it with a lint-free cloth.

After the source had been electroplated to the stainless steel substrate, it was fastened to two copper leads shown in Figure 19 on a ceramic backing by using two steel rectangular washers with dimensions 0.79 cm by 1.27 cm by 0.32 cm. This entire heating apparatus was subsequently secured inside a vacuum chamber. In addition, the current supply was modified so that the current readout was transmitted as an electrical signal that could be monitored by a voltage probe, providing a method with which the current could be recorded directly.

The chamber was pumped down to about $1 \cdot 10^{-6}$ Torr, which was measured using a cold cathode gauge, and the copper leads extending from the chamber were connected to a Mastech HY1550EX current supply. The current was turned up slowly to about 30A to heat up the foil to 1000°C for two hours to allow the source material to be absorbed into the lattice structure of the steel foil.

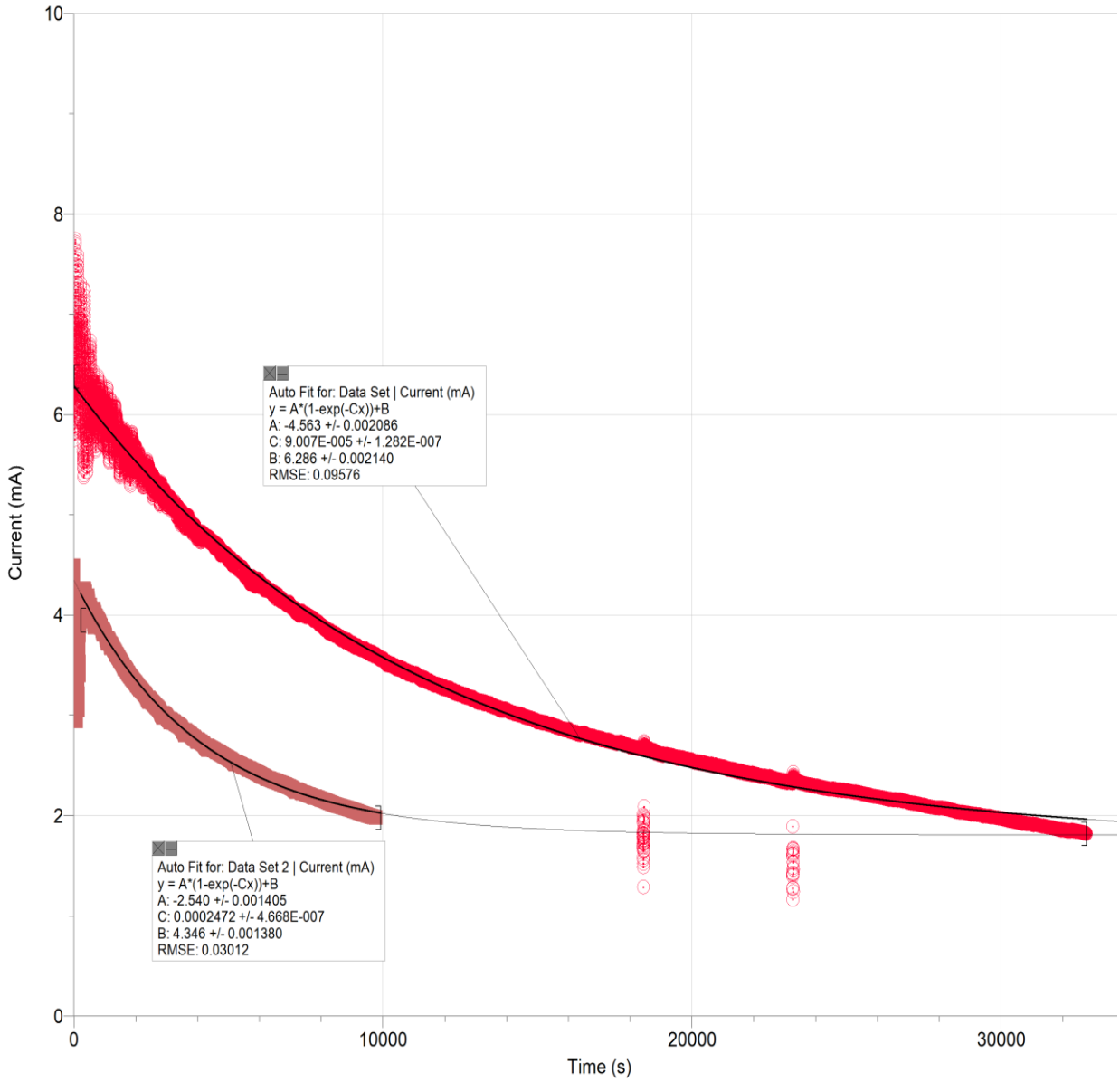

Figure 18: A typical plot of the electroplating current as a function of time. First, the HCl disassociation current (with no Cobalt ions) was collected (brown). Next, the electroplating current was collected (red), and both plots are fitted with a decaying exponential trend line. Notice that both fits approach nearly the same asymptote—this is estimated to be the 'base' HCl disassociation current. The two anomalies at approximately 18000 and 23000 seconds are from stirring the solution.

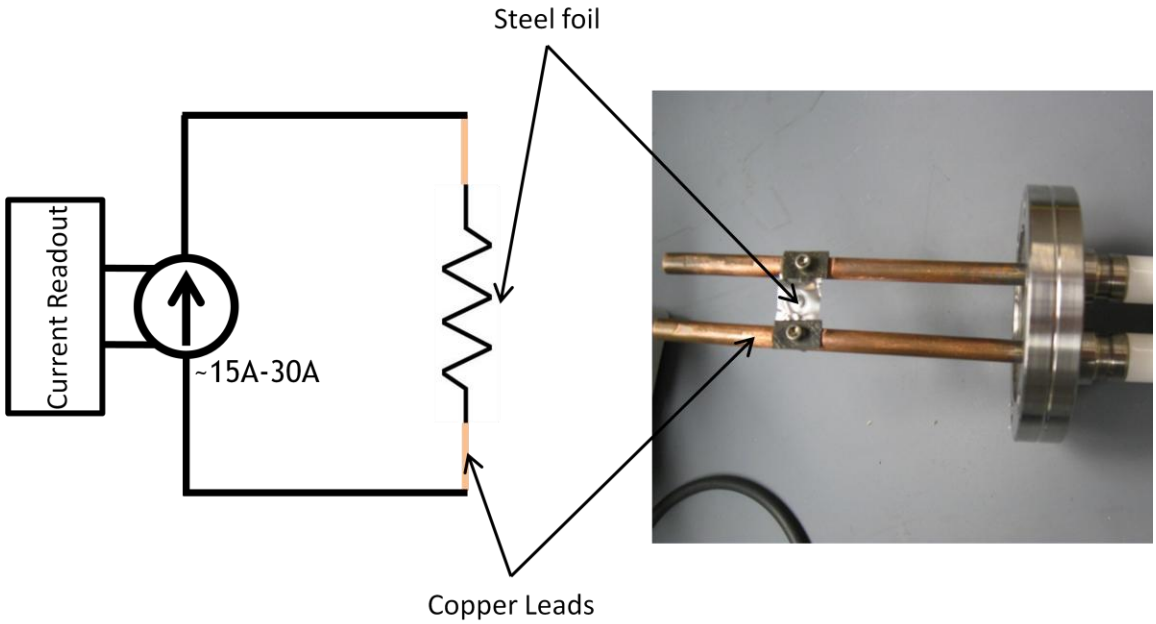

Figure 19: Photograph of the heating element with a circuit diagram. The stainless steel foil was secured between the two copper leads, and the variable current supply was used to control the foil's temperature.

3.2 The Vacuum Chamber

In order to complete the process for making a source, a vacuum chamber was constructed that was capable of reducing the pressure to less than one μTorr. The chamber consisted a number of standard 2.75 inch conflate tees, and was pumped down in two stages. A fore-pump, diffusion pump, and a cold trap, served to evacuate the chamber. Initially, the fore-pump was turned on until the pressure was on the order of 10^{-4} Torr, before turning on a Kurt J. Lesker TNR6XA150QF diffusion pump.

The diffusion pump consisted of a heating plate which heated a small amount of diffusion pump oil. The evaporating oil was forced through a series of jets, each of which redirected the oil so that it was pumped downward, producing the desired effect of evacuating the chamber. Moreover, a cold trap was placed directly above the diffusion pump. This was filled with liquid nitrogen so that any oil or water vapor that was not redirected by the baffles would come in contact with the cold trap and fall back down into the diffusion pump.

A butterfly valve, air release valve, Televac MP7ER cold cathode pressure gauge, and an ion gauge, were used to monitor and regulate the vacuum chamber. A butterfly valve proved to be necessary in order to close off the pumps so that other elements within the other regions of the chamber could be replaced. An ion gauge was added because it became apparent while using the vacuum chamber that the cold cathode gauge did not read pressures accurately once they approached one μTorr. Because the ion gauge measure higher air pressures ($> 10^{-4}$Torr), it was desirable to use s cold cathode gauge to determine the appropriate time to activate the ion gauge. Lastly, the air release valve was added so that the chamber could be brought back up to atmospheric pressure before attempting to dismantle other chamber components.

The experimental portion of the system included the heating element, thermocouples and viewing window, and was used to complete the heat treatment stage in the foil making process. The Omega K-type thermocouples were initially installed so that they could monitor the temperature of the foil and the chamber simultaneously. Even though it was known that the temperature of the foil measured by the thermocouple would not be its actual temperature, it was hypothesized that it would at least be a function to the real temperature. If this was the case, then a couple of different readings at known temperatures could be used in order to calibrate the temperature. However, it was found that the temperatures read by the thermocouple varied too little to derive an accurate calibration.

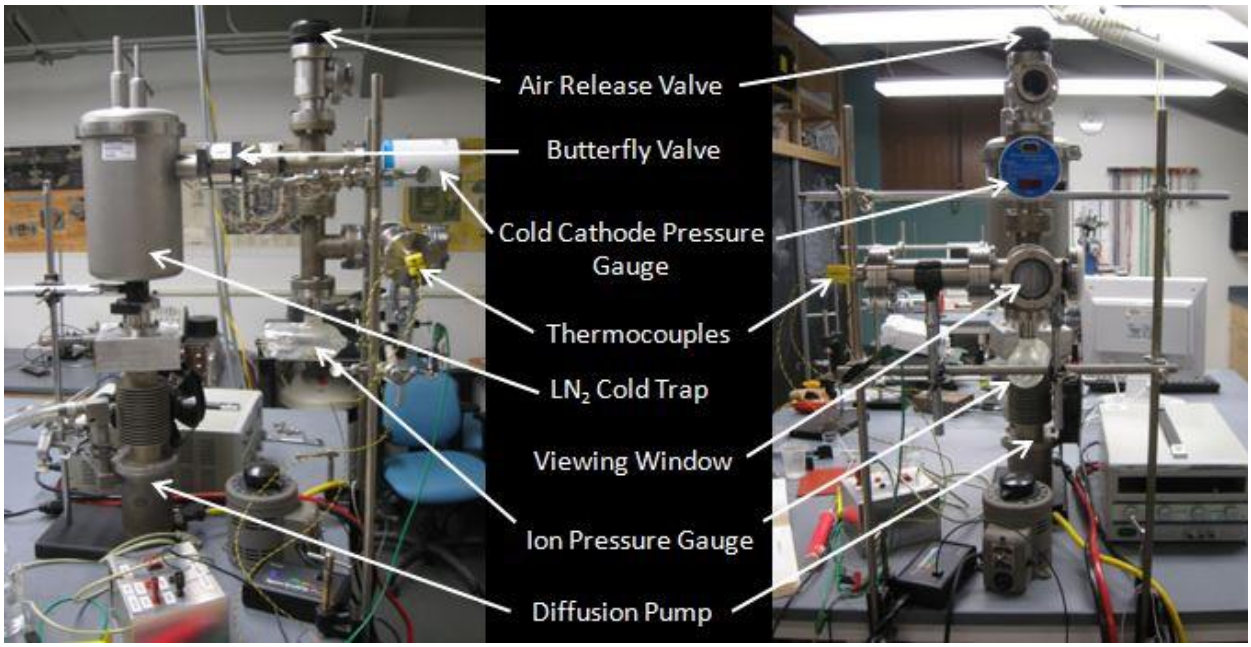

Figure 20: Two different perspectives of the vacuum chamber that the heating element was attached to (not shown in above figure). The vacuum chamber was first evacuated to approximately 10^{-6} Torr before heating the steel foil.

3.3 Analyzing the Source

The mass $m_{electroplated}$ of the $^{59}CoCl_2{\cdot}6H_2O$ electroplated to each foil was determined by measuring the mass of the foil to within one ten-thousandth of a gram after the electroplating process m_{final} and subtracting the initial mass of the foil $m_{initial}$ so that

$$m_{electroplated} = m_{final} - m_{initial} \tag{3.3.1}$$

In addition, the percentage of the ^{59}Co ions electroplated to foil was calculated by first finding the ratio of the mass of the ^{59}Co ions to the mass of the $^{59}CoCl_2{\cdot}6H_2O$, given that

$$m_{59CoCl2\cdot6H2O} = m_{Co} + 2(m_{Cl}) + 6[2(m_H) + m_O] = 237.923\ {}^{g}/_{mole}$$

$$m_{59Co} = 58.933\ {}^{\mathrm{g}}/_{\mathrm{mole}}. \qquad 3.3.2)$$

Then the mass of ^{59}Co ions within a given sample of $^{59}CoCl_2{\cdot}6H_2O$ of known mass was calculated by multiplying the ratio of the mass of the ^{59}Co ions to the mass of the $^{59}CoCl_2{\cdot}6H_2O$ by the mass of the $^{59}CoCl_2{\cdot}6H_2O$ sample. The amount of ^{59}Co ions present within the entire 0.1 M HCl solution was generally on the order of 10^{-2} g.

Before the $^{59}CoCl_2{\cdot}6H_2O$ was mixed into the HCl solution, a sample of about 5mL HCl was weighed. The difference in mass of the solution before and after the cobalt chloride was placed in the HCl allowed for the calculation of its mass.

After electroplating some of the ^{59}Co onto the foil, the mass of the $^{59}CoCl_2{\cdot}6H_2O$ and HCl solution was re-measured. By taking the difference of the mass of the solution before and after a portion of it was placed into the electroplating apparatus

$$m_{solution} = m_{solution\ before} - m_{solution\ after}, \qquad (3.3.3)$$

and by dividing it by the initial mass of the solution $m_{solution\ before}$, the fraction of the initial solution was determined. By assuming a homogeneous solution of $^{59}CoCl_2{\cdot}6H_2O$ and HCl, the mass of the available ^{59}Co ions, $m_{available}$ for the amount of cobalt chloride solution used was then be calculated by multiplying the ratio ${}^{m_{used}}/_{m_{solution\ before}}$ by the initial mass of the ^{59}Co ions present in the initial $^{59}CoCl_2{\cdot}6H_2O$ sample. Finally, the percentage of ^{59}Co electroplated to the foil was determined by

$$\%\ Electroplated = \frac{m_{electroplated}}{m_{available}} \qquad (3.3.4)$$

The percentage of ^{59}Co electroplated was checked by measuring the current as a function of time collected by the multi-meter and fit an exponentially decaying trend line of the form

$$I(t) = B - Ae^{-Ct}, \tag{3.3.5}$$

It can be seen in Figure 18 that as t becomes large, $I(t)$ approaches $(B + A)$. The physical manifestation of this relationship is apparent through the exponentially decaying ^{59}Co electroplating current $-Ae^{-Ct}$ combined with the relatively constant HCl and H_2O disassociation current B. Using this approximation, the percentage of ^{59}Co electroplated onto the foil was calculated by first determining the approximate charge of ^{59}Co ions electroplated.

$$Q_{electroplated} = \int_0^t I(t)dt \tag{3.3.6}$$

Where $I(t)$ is the trendline fit of the electroplating current as a function of time excluding the 'base' current B, and $'t'$ is the duration of the electroplating process. The total number of ions available within the solution was subsequently calculated by evaluating the same integral over all time, such that

$$Q_{available} = \int_0^\infty I(t)dt. \tag{3.3.7}$$

Finally, the approximate percentage of ^{59}Co ions electroplated to the foil was determined by evaluating the ratio $Q_{electroplated}/Q_{available}$. Typical results calculated by using this ratio can be found in Section 4.2.

3.4 Counting a ^{57}Co Mössbauer Source

Generally, the work on this experiment has been limited to the construction of 'dummy' sources using non-radioactive ^{59}Co. Obviously, these are not functional sources, but they were made in order to establish a process for making 'real' Mössbauer sources. Once this has been accomplished, the amount of ^{57}Co deposited onto the stainless steel foil could be approximated by measuring the level of radioactivity through a relatively simple process. First, the amount of ^{57}Co that is to be electroplated onto the foil will be dissolved into an electroplating solution in a process similar to the one described in Section 3.1. The volume of the solution that the cobalt will be dissolved in will be equal to the

capacity of the glass tee. This solution will be placed into a wide, open container to spread out the liquid in a way that allows the geometry of the solution to be as close to the contour of the electroplated source as possible. Next, this container will be placed a fixed distance from a Geiger counter so that the radioactivity of the solution can be determined. After electroplating the cobalt mixture, the foil can be counted by placing the detector the same distance away from the source and for the same duration as what was done with the solution prior to electroplating. Using this data, the mass of the cobalt deposited onto the foil can be determined by multiplying the fraction of the cobalt that was successfully electroplated by the initial mass of the ^{57}Co.

3.5 Detecting the Mössbauer Effect

It is hoped that around 5μC of ^{57}Co will be successfully electroplated and baked into a steel substrate in order to make a functional Mössbauer source.

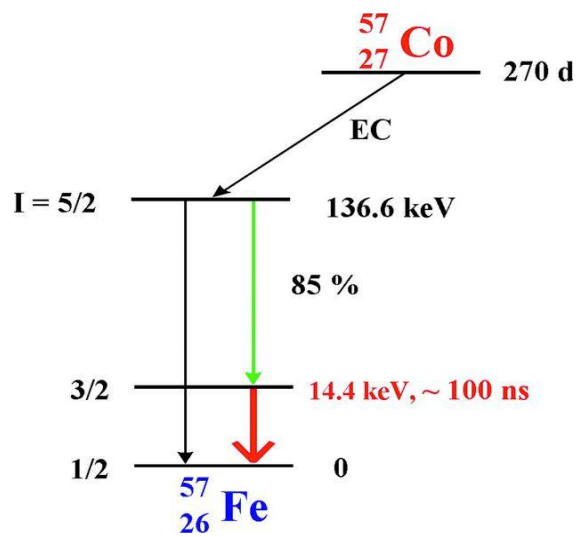

Figure 21: Decay scheme for ^{57}Co. The cobalt decays into an excited state of ^{57}Fe through electron capture nearly 100% of the time. For this project, the portion of the decay chain that is of interest is from the 136.5 keV to 14.4 keV to ground state transition. This particular transition has an 85% chance of occurring and results in a 14.4 keV gamma ray being emitted directly after a 122 keV photon. Figure taken from Ref. [15].

Notice in Figure 21 that eighty-five percent of the time when ^{57}Co decays into an excited state of ^{57}Fe, it transitions into the ground state by emitting a 14.4 keV gamma ray in coincidence with a 122 keV gamma ray. The 122 keV photon can be used to trigger a gate which allows the 14.4 keV gamma ray to be subsequently detected, as shown in Figure 22. By detecting the 14.4keV gamma ray in this fashion, the number of background counts can be greatly reduced, because the gate will only be opened during for times when 14.4 keV gamma rays from the source are emitted.

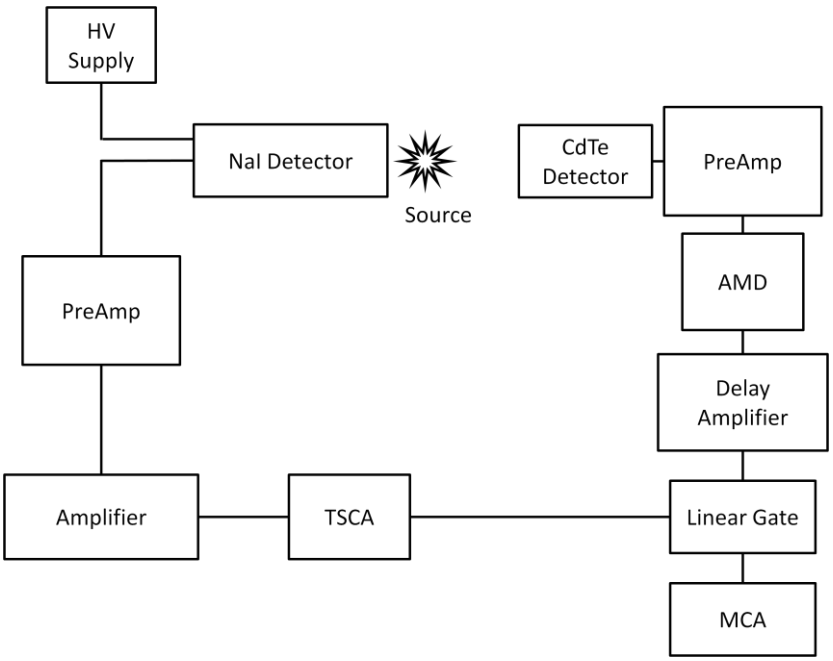

Figure 22: Proposed circuit diagram for detection apparatus. When a high-energy photon is detected, the sodium-iodide detector emits a pulse. The timing single-channel analyzer (TSCA) is used to isolate the energies immediately around 122keV. If this condition is met, a logic pulse is sent to the linear gate, which allows the pulse emitted by the X-ray detector at that time to be collected by the multi-channel analyzer (MCA). Giving that the only gamma rays that are to be collected as events are 14.4 keV gamma rays immediately following the detection of a 122 keV gamma ray, this circuit setup should greatly reduce the number of background counts.

This is another reason why ^{57}Co is desirable to use as a Mössbauer source for the two proposed experimental setups described earlier.

Chapter 4

RESULTS AND SETBACKS

4.1 Count Rate Estimates

Before this experiment could begin, it was necessary to determine whether or not small exempt radioactive sources could be used as viable Mössbauer sources. To answer this question, count rate estimates were made by using MathCAD to obtain high enough count rates to be useful for expected source activity, as well as apparatus and detector parameters that were relevant to the experiment. When this was done, it was determined that if a 5μC, ^{57}Co source is used in our apparatus, approximately 519 counts could be detected over a period of one hundred seconds, giving a statistical uncertainty of just over four percent. From these calculations, it was concluded that in theory, a useable Mössbauer source could be made using exempt radioactive sources. (For detailed calculations, see Appendix B).

4.2 Electroplating

One of the biggest obstacles to overcome when the source material (^{59}Co or ^{57}Co) was being electroplated to the steel foil was measuring exactly how much of it was successfully electroplated. Unfortunately, the two different methods of measuring the amount of cobalt electroplated to the steel; namely, integrating the electroplating current as a function of time and weighing the foil before and after each run (as discussed in Section 3.3), often disagreed with one another by a significant amount.

Table 4: A table comparing the two different methods used for calculating the percentage of cobalt that was electroplated onto the steel foil for the four different electroplating runs. The methods for calculating each percentage value are explained in detail in Section 3.2. For the initial conditions used to calculate these percentages, see Appendix C.

	% Electroplated (Mass)	% Electroplated (Calculated)	% Difference	Duration of Electroplating
Run 1	74	98	24	3.03 hr
Run 2	64	84	20	3.26 hr
Run 3	98	99	1	5.24 hr
Run 4	92	98	6	6.05 hr

Notice that in general, as the duration of the electroplating process increases, the discrepancy between the two methods of measuring the percentage of the cobalt ions electroplated to the foil decreases, even though both methods should have measured an equal percentage of the available cobalt electroplated to the foil. However, it was noticed that the current would greatly fluctuate as soon as the current was turned on, and continued to do so for around half an hour (evidence of this can be seen in Figure 18). Though this effect averages out over time, the trend line may have been inaccurate for shorter runs because the recorded data set was not large enough to offset initial fluctuations.

4.3 Measuring the Foil Temperature

As mentioned in Section 1.3, a foil has to be heated to around 1000ºC for two hours in order for the source material to diffuse into the lattice structure of the foil. A major difficulty that was encountered during the heating process was determining the temperature of the foil. Two different approaches were taken to measure the temperature: using the resistivity of the foil as a function of temperature and measuring the blackbody spectrum of the foil.

The relationship between resistance and resistivity for a rectangular foil is given by

$$\rho = \frac{RtW}{L} \tag{4.3.1}$$

where ρ is the resistivity, R is resistance, t is the thickness of the foil, W is its width, and L is the foil's length.

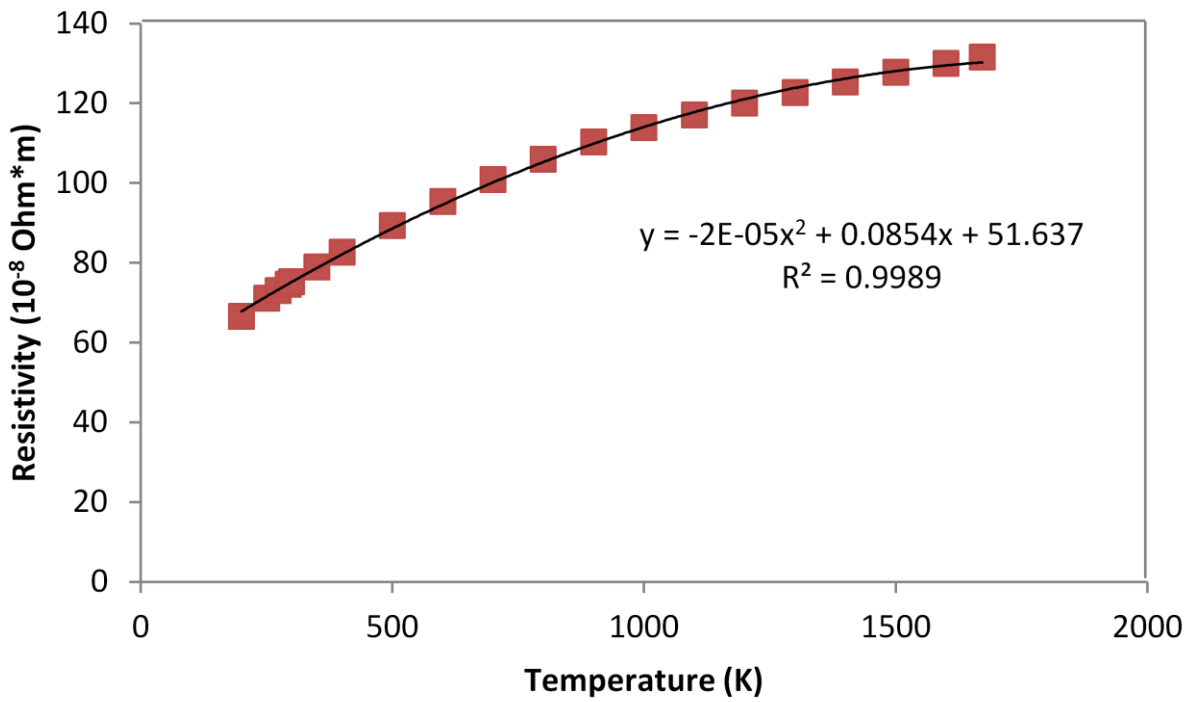

Figure 23: A plot of the resistivity as a function of temperature for 321 grade stainless steel for temperatures ranging from 200 K to 1672 K (melting point of steel). Using Excel, a quadratic trend line was fit to the published data. The formula for this trend line, as well as the R^2 value for this fit, is shown in the above graph.

The foil used in this experiment was had the dimensions shown in Section 2.2; however, because the lengths of the rectangular washers were made L = W, then the above equation can be simplified to

$$\rho = Rt. \tag{4.3.2}$$

This assumes that the resistance of the washers is negligible in comparison to the resistance of the foil such that the current flows only through the portion of the foil that is not anchored under the washers. This should be a viable assumption, as the thickness of the washers was about sixty times that of the foil. In order to measure the temperature of the foil using this method, the current flowing through the foil, as well as the potential difference across the two copper electrodes were monitored using the current and voltage readouts on the display of the current supply. Because the resistance of the rest of the heating apparatus was small in comparison to the resistance of the foil and because the cross-sectional area of the copper leads was about two orders of magnitude larger than that of the foil, the resistance of the rest of the heating apparatus was considered to be approximately constant with increasing current. Using this approximation, the resistance of the entire apparatus was calculated using Ohm's Law. A small amount of current was run through the apparatus, and the electrical potential between the two leads (measured using a multi-meter) was divided by the current. This process was repeated for currents ranging from one to five Amps, and the final result was calculated by averaging all of the individual measurements, giving a total resistance of 10 mΩ. In addition, the resistance of the foil was calculated by subtracting the resistance of the apparatus from the measurement of the total resistance. By using the dimensions of the foil, the resistivity was determined. These different resistivity values were tabulated alongside the corresponding voltage and current values (an example of this is shown in Appendix D). In order to determine the temperature using the resistivity, the measured data was normalized to the published values [16] by using the resistivity of the foil at room temperature. The approximate temperature of the foil could then be determined by using the normalized plot of resistivity as a function of temperature. By using this method, it was determined that the desired temperature was reached when the current flowing through the foil was at approximately 30 A. The result is shown in Figure 24.

The second way that the temperature was determined was by fitting a blackbody curve to the measured emitted light spectrum. A Spectrum Techniques LLC light sensor was taped to the viewing window of the vacuum chamber and surrounded by aluminum foil to block out as much external light

as possible. Next, the light spectrum as a function of wavelength for each current setting, and Minuit [18] was used to make a blackbody fit of the emitted light spectrum by using Planck's Law for blackbodies, given by

$$P(\lambda, T) = \frac{2\pi hc^2}{\lambda^5 \left(e^{hc/kT} - 1\right)}$$

where P(λ,T) is the power radiated per unit area per unit wavelength at temperature T. The approximate temperature of the foil could then be determined using Wien's Law.

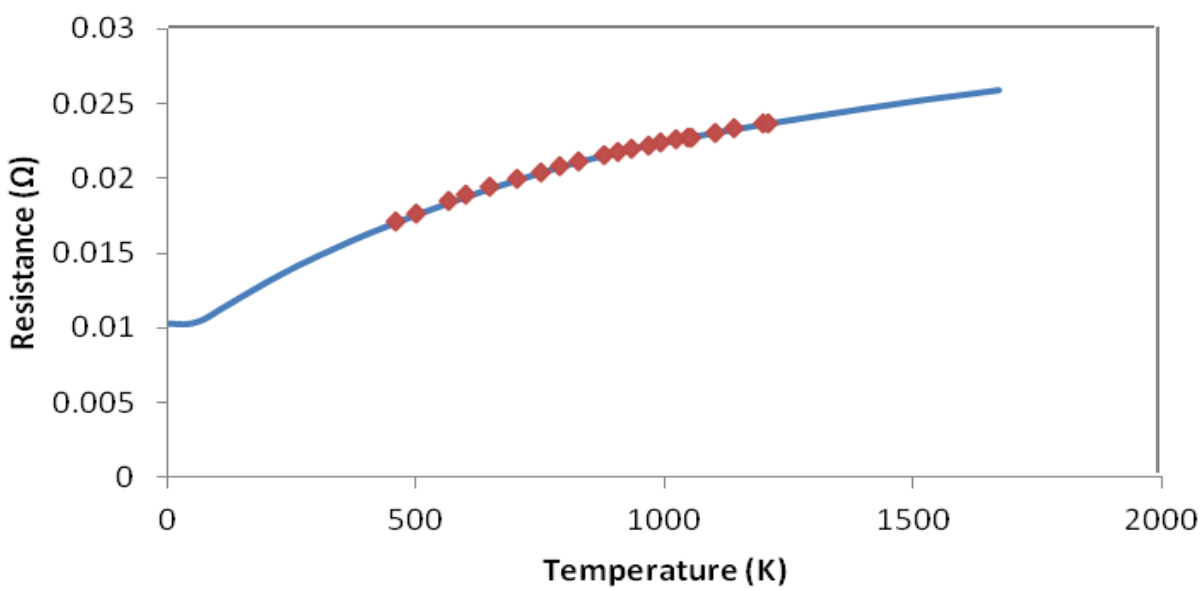

Figure 24: Plot of the resistance of the foil as a function of temperature using the published values [16] for 321 grade stainless steel (line) and the measured resistance of the foil for different currents (points). The theory line was calculated by using the published values for the resistivity of stainless steel as a function of temperature with the dimensions for the foil used. The recorded values were normalized to the theory curve at room temperature in order to compare the measured resistance with the published data set.

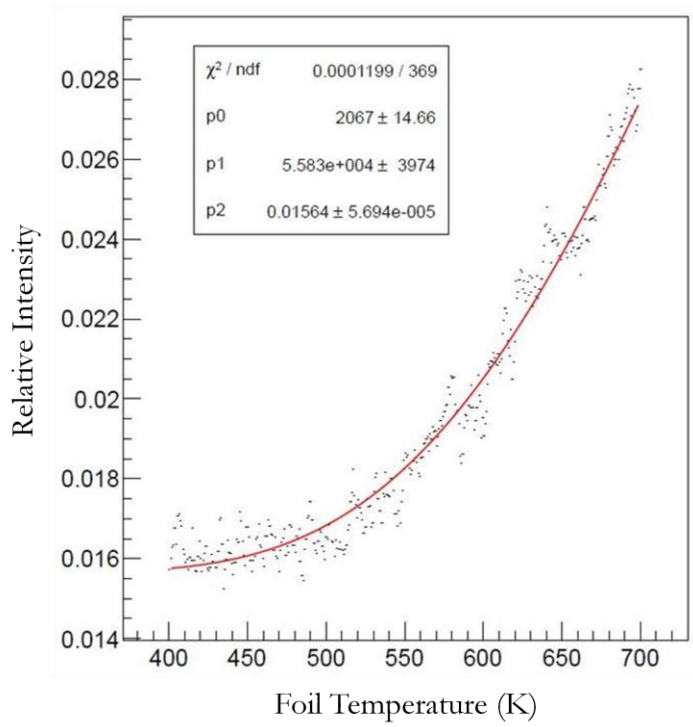

Figure 25: Blackbody fit of the light spectrum emitted from the foil at a current of 32 A. The fit was made using Minuit [18] The peak of this particular blackbody spectrum is given in Kelvin by the p0 parameter.

As it can be seen in Figure 25, the calculated value of the foil temperature using the blackbody fit was about 400 K greater than the melting point [16] of 321 grade stainless steel. Since the steel foil remained intact throughout the entire heating process, it was inferred that this particular measurement was too high by at least that amount. Unfortunately though, no other blackbody measurements have been carried out, so additional investigation into this particular method would be necessary in order to determine whether or not it can be used to measure the temperature of the foil.

One possible explanation for why the blackbody fit was off by such a large amount could be because the emitted spectrum of the foil was different than the spectrum that was measured by the light sensor. For example, if the vacuum chamber viewing window absorbed a significant fraction of the infrared portion of the spectrum (as most types of glass do), the peak wavelength of the foil would shift

upward to higher frequencies, which would cause the peak measurement to be skewed towards higher temperatures. In addition, there was occasionally a noticeable film of steel deposited on the inside of the viewing window as the result of emission of ions from the heated foil. Although this buildup was cleaned periodically by scrubbing the inside of the viewing window with alcohol, the presence of metal ions left on the inside of the glass could have contributed to the reflection of certain wavelengths of light that further skewed the spectrum that was detected by the light sensor. In the future, if possible, the light sensor should be inside the vacuum chamber positioned in front of the foil to see if the measured blackbody peak is closer to the predicted value for each resistance.

Chapter 5

FUTURE PLANS AND CONCLUSION

A few assessments can be made regarding progress up to this point. According to the count rate estimates discussed in Section 3.5, it is theoretically possible to make a viable Mössbauer source using exempt sources. As of yet, "imitation" sources have been successfully constructed using ^{59}Co so that the process of making a Mössbauer source has been established. It has been decided that for the purposes of this project, ^{57}Co is the appropriate gamma emitter for use in the construction of Mössbauer sources. Finally, future plans include using these Mössbauer sources to investigate the longitudinal Doppler shift, as well as to test general relativity using the transverse Doppler effect.

Appendix A

DIFFERENT MÖSSBAUER ABSORBERS AND THEIR PROPERTIES

The following table depicts several different nuclei by which the Mössbauer Effect has been observed. [17]

a = Abundance of the element as a percentage of all of its known isotopes

Q = Ratio of the transition energy E_γ to the line width $\Gamma = \hbar \ln\left(\frac{2}{T_{1/2}}\right)$

R = Energy lost by the gamma ray to a single emitter nucleus due to recoil (10^{-2} eV)

$\sigma_o{}'$ = Mössbauer absorption cross section in units of 10^{-19} cm^2

T½ = Mean lifetime of excited state in seconds

Nuclide	a	Eγ	T 1/2	Q	R	σo'
	%	keV	seconds		1E-2 eV	1E-19 (cm^2)
57Fe	2.17	14.4	1.00E-07	3.20E+12	0.19	22.6
61Ni	1.25	71	5.20E-09	8.10E+11	4.4	6.6
67Zn	4.11	93	9.40E-06	1.90E+15	6.9	1.2
83Kr	11.55	9.3	1.50E-07	3.10E+12	0.055	21
107Ag	51.35	93	4.43E+01	9.00E+21	4.3	0.67
119Sn	8.58	24	1.90E-08	1.00E+12	0.26	1.7
123Sb	42.75	161	6.00E-10	2.10E+11	11	0.71
125Te	6.99	35	1.60E-09	1.20E+11	0.52	3.1
129I	unstable	26.8	1.85E-08	1.10E+12	0.3	25.6
129Xe	26.44	40	7.00E-10	6.20E+10	0.67	30
149Sm	13.8	22	>2.8E-9	n/a	0.17	n/a
151Eu	47.77	22	9.50E-09	4.50E+11	0.17	5.2
155Gd	14.7	87	n/a	n/a	2.6	2.3
160Dy	2.294	87	1.80E-09	3.40E+11	2.6	6.4
161Dy	18.88	25.7	2.80E-08	1.60E+12	0.22	37
161Dy	18.88	74.5	3.00E-09	4.90E+11	1.80E+00	2.00E+00
166Er	33.4	80	1.80E-09	3.20E+11	2.1	7.1
169Tm	100	8.4	4.00E-09	7.40E+10	0.022	700
170Yb	3.03	84.2	1.57E-09	2.90E+11	2.2	6.6
177Hf	18.5	113	4.20E-10	1.00E+11	3.9	1.4
182W	26.4	100	1.30E-09	2.90E+11	2.9	2.2
183W	14.4	46.5	n/a	n/a	0.63	2.3
183W	14.4	99.1	5.20E-10	1.10E+11	2.9	1.7
187Re	62.93	134	2.00E-09	5.90E+11	5.2	0.58
191Ir	38.5	129	1.40E-10	4.00E+10	4.7	0.56
193Ir	61.5	73	6.00E-09	9.60E+11	1.5	2.3
195Pt	33.8	99	1.40E-10	3.00E+10	2.7	0.5
195Pt	33.8	129	5.50E-10	1.60E+11	4.6	4.4
197Au	100	77	1.90E-09	3.20E+11	1.6	0.59

Appendix B

COUNT RATE ESTIMATES FOR ^{57}CO

Before beginning the experiment, the approximate count rate expected from a small exempt ^{57}Co source was calculated, in order to determine whether or not such a source would be useful for our purposes. This count rate estimate was compared to the count rates of other experiments where ^{57}Co was used using the same calculation process. All calculations were made using MathCAD software [19].

MOSSBAUER EXPERIMENT

General Constants

Units	$fm := 10^{-15}\ m$	$MeV := 1.602 \cdot 10^{-13}\ J$	$keV := \frac{MeV}{1000}$
	$\mu m := 10^{-6}\ m$		
	$barn := 10^{-28}\ m^2$	$Na = 6.022 \cdot 10^{23} \frac{1}{mole}$	
	$Ci := 3.7 \cdot 10^{10} \cdot sec^{-1}$		
electron radius	$r_0 = 2.82\ fm$	$2 \cdot \pi \cdot (r_0)^2 = 0.5 \cdot barn$	
mass of electron	$me := 0.511\ MeV$		

Iron Properties

Density $\rho := 7.87 \frac{gm}{cm^3}$

Atomic mass/number $A := 55.845 \frac{gm}{mole}$ $Z := 26$

Number target atoms $Nt := \frac{Na}{A} \cdot \rho$ $Nt = 8.487 \cdot 10^{28} \frac{1}{m^3}$

Atomic Number $Z = 26$ electrons/iron atom

Iron attenuation coefficients

$$E := \begin{bmatrix} 0.01 \\ 0.02 \\ 0.03 \\ 0.04 \\ 0.05 \\ 0.06 \\ 0.08 \\ 0.1 \\ 0.2 \\ 0.3 \\ 0.4 \\ 0.5 \\ 0.6 \\ 0.8 \\ 1.0 \\ 1.25 \\ 1.5 \\ 2 \\ 3 \\ 4 \end{bmatrix} \qquad \mu := \begin{bmatrix} 1.706 \cdot 10^2 \\ 2.568 \cdot 10^1 \\ 8.176 \\ 3.629 \\ 1.958 \\ 1.205 \\ 0.5952 \\ 0.3717 \\ 0.1460 \\ 0.1099 \\ 9.4 \cdot 10^{-2} \\ 8.414 \cdot 10^{-2} \\ 7.704 \cdot 10^{-2} \\ 6.699 \cdot 10^{-2} \\ 5.995 \cdot 10^{-2} \\ 5.350 \cdot 10^{-2} \\ 4.883 \cdot 10^{-2} \\ 4.265 \cdot 10^{-2} \\ 3.621 \cdot 10^{-2} \\ 3.312 \cdot 10^{-2} \end{bmatrix}$$

Give correct units

$EE = E \cdot MeV$

$\mu\mu := \mu \cdot \frac{cm^2}{gm}$

Air Properties

Density $\rho a := 1.2754 \frac{kg}{m^3}$ At 20 °C and 101.325 kPa, dry air has a density of 1.2041 kg/m3.

Air attenuation coefficients

$$Ea := \begin{bmatrix} 0.01 \\ 0.02 \\ 0.03 \\ 0.04 \\ 0.05 \\ 0.06 \\ 0.08 \\ 0.1 \\ 0.2 \\ 0.3 \\ 0.4 \\ 0.5 \\ 0.6 \\ 0.8 \\ 1.0 \\ 1.25 \\ 1.5 \\ 2 \\ 3 \\ 4 \end{bmatrix} \qquad \mu a := \begin{bmatrix} 5.12 \\ 0.7779 \\ 0.3538 \\ 0.2485 \\ 0.208 \\ 0.1875 \\ 0.1662 \\ 0.1541 \\ 0.1233 \\ 0.1067 \\ 9.549 \cdot 10^{-2} \\ 8.712 \cdot 10^{-2} \\ 8.055 \cdot 10^{-2} \\ 7.074 \cdot 10^{-2} \\ 6.358 \cdot 10^{-2} \\ 5.687 \cdot 10^{-2} \\ 5.175 \cdot 10^{-2} \\ 4.447 \cdot 10^{-2} \\ 3.581 \cdot 10^{-2} \\ 3.079 \cdot 10^{-2} \end{bmatrix}$$

Give correct units

$EEa := Ea \cdot MeV$

$\mu\mu a := \mu a \cdot \frac{cm^2}{gm}$

Number of gammas counted

gamma det solid angle fraction

$$SAg(distance, area) := \frac{area}{(distance^2)} \cdot \frac{1}{4 \cdot \pi}$$

gamma det of radius is dist from source

Area of detector

$$Area(det\_radius) := \pi \cdot det\_radius^2$$

Number incident (number detected w/o absorber + air)

$$N0(activity, distance, area, time, effg) := activity \cdot SAg(distance, area) \cdot time \cdot effg$$

Abs coef for air

$$\rho a(energy) := (linterp(EEa, \mu\rho a, energy)) \cdot \rho a$$

Abs coef for iron

$$\mu(energy) := linterp(EE, \mu\rho, energy) \cdot \rho$$

Air attenuation

$$atten\_air(distance, energy) := \exp(-\mu a(energy) \cdot distance)$$

Iron attenuation

$$atten\_iron(thickness, energy) := \exp(-\mu(energy) \cdot thickness)$$

Total number transmitted

$$NN(activity, distance, thickness, area, effg, energy, time) := N0(activity, distance$$

Test Values (Bearden et al)

Acquisition time	$T0 := 1\ sec$	
source to detector distance	$L0 := 11\ cm$	
Thickness of absorber	$X0 := 0.0005 \cdot in$	
Gamma energy	$E0 := 14\ keV$	
Activity of source	$A0 := 1 \cdot 10^{-3} \cdot Ci$	
Area of detector	$S0 := 1.613 \cdot cm^2$	
Gamma det efficiency	$Effg := 0.85 \cdot 0.95 \cdot 0.95$	gamma det 85% eff two 1/16 in plexiglass
Number incident (number detected w/o absorber + air)	$N0(A0, L0, S0, T0, Effg) = 3.011 \cdot 10^4$	
Abs coef for air	$\mu a(E0) = 0.431\ \frac{1}{m}$	
Abs coef for iron	$\mu(E0) = 8.864 \cdot 10^4\ \frac{1}{m}$	
Air attenuation	$atten\_air(L0, E0) = 0.954$	
Iron attenuation	$atten\_iron(X0, E0) = 0.324$	
Total number transmitted	$NN(A0, L0, X0, S0, Effg, E0, T0) = 9.315 \cdot 10^3$	

Test Values (Scorza et al)

Acquisition time	$T0 := 1\ sec$
source to detector distance	$L0 := 20\ cm$
Thickness of absorber	$X0 := 25 \cdot \mu m$
Gamma energy	$E0 := 14\ keV$
Activity of source	$A0 := 1 \cdot 10^{-3} \cdot Ci$
Area of detector	$S0 := 1 \cdot cm^2$
Gamma det efficiency	$Effg := 0.35$
Number incident (number detected w/o absorber + air)	$N0(A0, L0, S0, T0, Effg) = 2.576 \cdot 10^3$
Abs coef for air	$\mu a(E0) = 0.431 \frac{1}{m}$
Abs coef for iron	$\mu(E0) = 8.864 \cdot 10^4 \frac{1}{m}$
Air attenuation	$atten\_air(L0, E0) = 0.917$
Iron attenuation	$atten\_iron(X0, E0) = 0.109$
Total number transmitted	$NN(A0, L0, X0, S0, Effg, E0, T0) = 257.697$ measured = 225 (400 moving)

Our Experiment

Acquisition time	$T0 := 100\ sec$
source to detector distance	$L0 := 10\ cm$
Thickness of absorber	$X0 := 0.001 \cdot in$
Gamma energy	$E0 := 14\ keV$
Activity of source	$A0 := 5 \cdot 10^{-6} \cdot Ci$
Area of detector	$S0 := 1 \cdot cm^2$
Gamma det efficiency	$Effg := 0.35$

Number incident (number detected w/o absorber + air)	$N0(A0, L0, S0, T0, Effg) = 5.153 \cdot 10^3$
Abs coef for air	$\mu a(E0) = 0.431\ \frac{1}{m}$
Abs coef for iron	$\mu(E0) = 8.864 \cdot 10^4\ \frac{1}{m}$
Air attenuation	$atten\_air(L0, E0) = 0.958$
Iron attenuation	$atten\_iron(X0, E0) = 0.105$
Total number transmitted	$NN(A0, L0, X0, S0, Effg, E0, T0) = 519.374$

Note: measure BG with NaI=297 in 100 sec

Uncertainty	$\sqrt{NN(A0, L0, X0, S0, Effg, E0, T0)} = 22.79$
Fractional	$\frac{\sqrt{NN(A0, L0, X0, S0, Effg, E0, T0)}}{NN(A0, L0, X0, S0, Effg, E0, T0)} = 4.388 \cdot \%$

Needs to be better than 20%

Appendix C

CALCULATING THE PERCENTAGE OF ^{59}CO ELECTROPLATED

The following information was used to calculate the percentage of the ^{59}Co that was available in the solution that was successfully electroplated onto the stainless steel substrate.

	mass electroplated	59Co Available	Solution Used	Total 59Co Mass	Total Solution Mass
Run 1	0.0045 g	0.0061 g	0.6600 g	0.0308 g	3.4905 g
Run 2	0.0037 g	0.0058 g	0.6656 g	0.0308 g	3.4905 g
Run 3	0.0046 g	0.0047 g	0.5324 g	0.0308 g	3.4905 g
Run 4	0.0051 g	0.0056 g	0.6308 g	0.0308 g	3.4905 g

The values in the above table were used in the calculations described in Section 3.3 in order to determine what percentage of ^{59}Co ions available within the solution were electroplated to the foil depicted in Table 3.

The following plots depict the current as a function of time for the duration of each of the four electroplating runs in Table 3. The electroplating runs which they correspond to have been labeled, in addition to the trend line fit and collection time in seconds.

Run1: $I(t) = 5.873e^{-0.0001762t} + 0.688, \quad 0 < t < 21794$

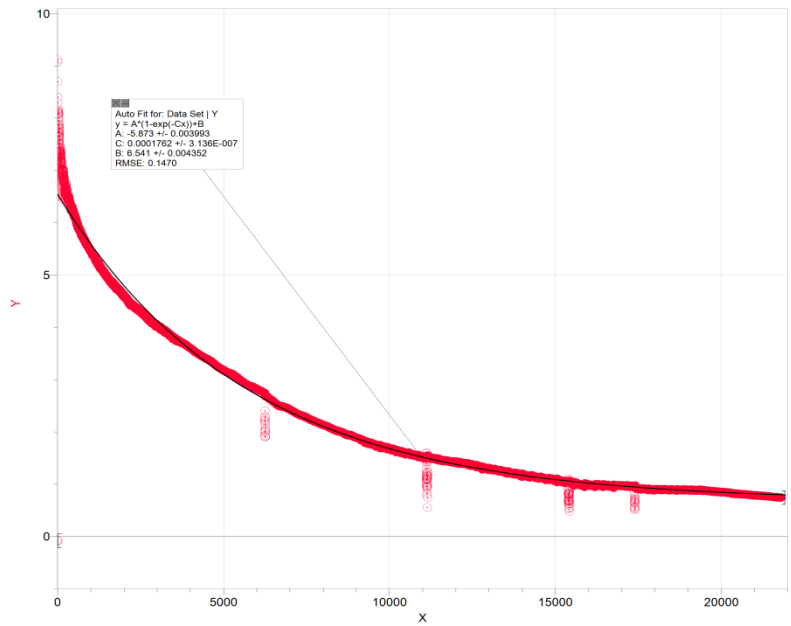

Run 2: $I(t) = 3.671e^{-0002628t} + 2.225, \quad 0 < t < 11747$

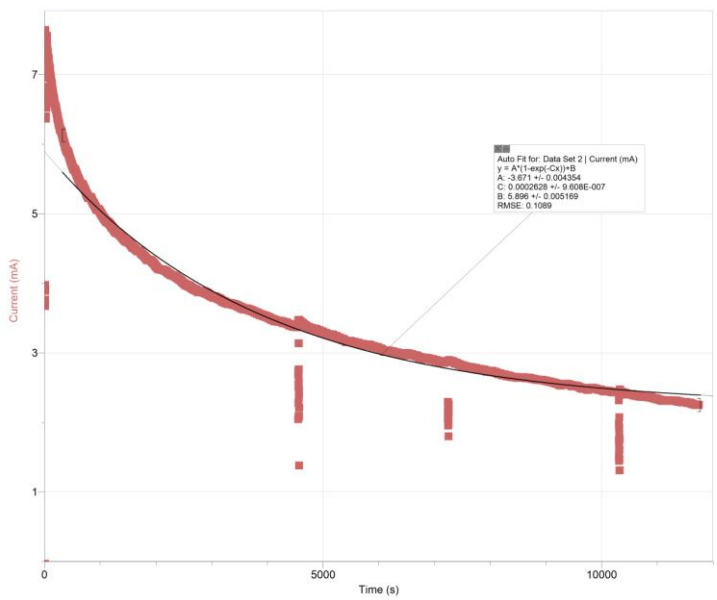

Run 3: $I(t) = 4.556e^{-0002285t} + 1.679, \quad 0 < t < 18864$

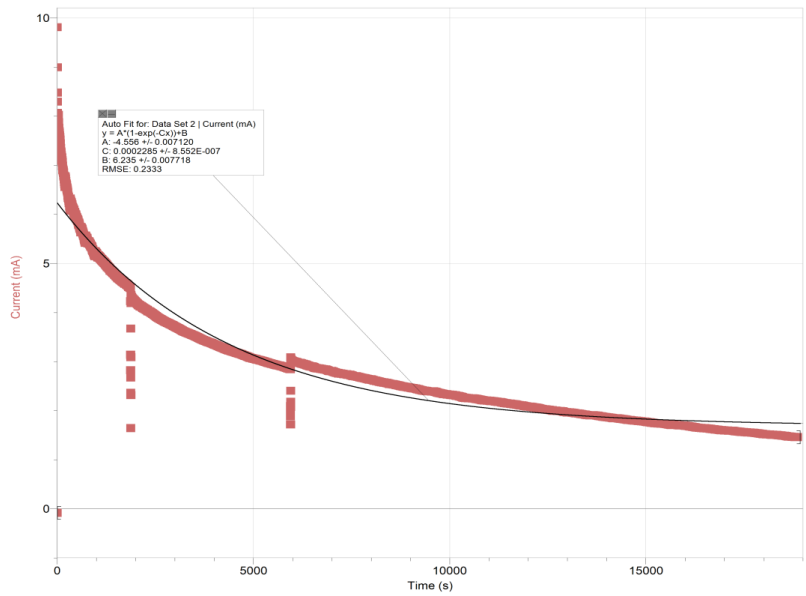

Run 4: $I(t) = 5.872e^{-000.1762t} + 0.670, \quad 0 < t < 21793$

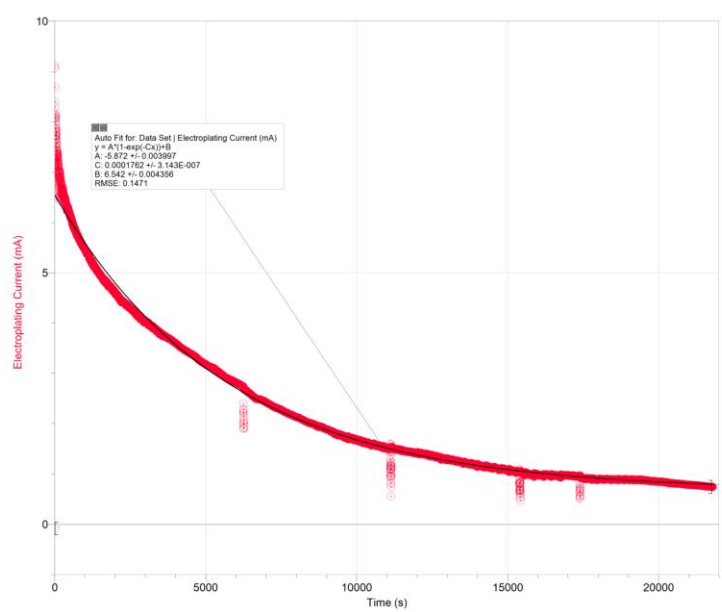

Appendix D

TYPICAL RESISTIVITY MEASUREMENT USING OHM'S LAW

Potential (V)	Current (A)	Resistance (Ω)	Resistivity (Ω*m)
0.2899	10	0.02899	1.47269E-06
0.3252	11	0.029563636	1.50183E-06
0.3646	12	0.030383333	1.54347E-06
0.4	13	0.030769231	1.56308E-06
0.4383	14	0.031307143	1.5904E-06
0.4781	15	0.031873333	1.61917E-06
0.517	16	0.0323125	1.64148E-06
0.5551	17	0.032652941	1.65877E-06
0.5935	18	0.032972222	1.67499E-06
0.6344	19	0.033389474	1.69619E-06
0.6722	20	0.03361	1.70739E-06
0.7101	21	0.033814286	1.71777E-06
0.7495	22	0.034068182	1.73066E-06
0.7871	23	0.034221739	1.73846E-06
0.8266	24	0.034441667	1.74964E-06
0.865	25	0.0346	1.75768E-06
0.9006	26	0.034638462	1.75963E-06
0.9434	27	0.034940741	1.77499E-06

The above values represent a typical data set that would be used to calculate the temperature of the foil. The potential and current flowing through the foil were collected by using the voltage and current readout on the current supply. By using $V = IR$, the resistance of the foil was calculated, and by using Equation 3.2.2, the resistivity was determined.

References

[1] R. W. Wood, *Philos. Mag.,* 6th Series, 1903, **6**, 362.
[2] W. Kuhn, *Philos. Mag.,* 1929, **8**, 635.
[3] P. B. Moon, *Proc. Phys. Soc.*, 1951, **64**, 76.
[4] K. G. Malmfors, *Arkiv för Fysik*, 1952, **6**, 49.
[5] R. Mössbauer, *Zeitschrift für Physik A* 1958, **151**, 124
[6] Kundig Phys Rev **129** 2371 (1963).
[7] Pound and Rebka Phys Rev Lett **4** 337 (1960).
[8] Kholmetskii et. al. NIM B **108** 359 (1996).
[9] Mustachi et. al. NIM **26** 219 (1964).
[10] Stephen NIM **26** 269 (1964).
[11] Qaim et. al. Jour Phys C **1** 1388 (1968).
[12] Weichang et. al. Int. J. Radiat. Appl. Instrum. A **41** 783, (1990).
[13] Bearden et. al. AJP **32** 109 (1964).
[14] Sconza Eur J Phys **11** 343 (1990).
[15] http://geea.lyellcollection.org/content/11/2/129/F5.expansion.html
[16] C. Y. Ho and T. K. Chu "Electrical Resistivity and Thermal Conductivity of Nine Selected AISI Stainless Steels" CINDAS Thermophysical Properties Research Center (1977)
[17] Frauenfelder, Hans. Chapters 1-2 *The Mössbauer Effect*, S.l.: W A Benjamin Inc, 1963.
[18] Rene Brun and Fons Rademakers, *ROOT - An Object Oriented Data Analysis Framework*, Proceedings AIHENP'96 Workshop, Lausanne, Sep. 1996, Nucl. Inst. & Meth. in Phys. Res. A 389 (1997) 81-86.
[19] Parametric Technology Corporation, *MathCAD 14.0.*, June 2008